NAVAL POSTGRADUATE SCHOOL
Monterey, California

THESIS

THERMAL ANALYSIS OF PANSAT

by

Travis R. Smith

December, 1997

Thesis Advisor:	Oscar Biblarz
Thesis Co-Advisors:	Ashok Gopinath
	Dan Sakoda

REPORT DOCUMENTATION PAGE

Form Approved OMB No. 0704-0188

1. AGENCY USE ONLY *(Leave blank)*	2. REPORT DATE	3. REPORT TYPE AND DATES COVERED
	Dec 1997	Master's Thesis

4. TITLE AND SUBTITLE
THERMAL ANALYSIS OF PANSAT

5. FUNDING NUMBERS

6. AUTHOR(S)
Smith, Travis, R.

7. PERFORMING ORGANIZATION NAME(S) AND ADDRESS(ES)
Naval Postgraduate School
Monterey, CA 93943-5000

8. PERFORMING ORGANIZATION REPORT NUMBER

9. SPONSORING / MONITORING AGENCY NAME(S) AND ADDRESS(ES)

10. SPONSORING / MONITORING AGENCY REPORT NUMBER

11. SUPPLEMENTARY NOTES
The views expressed in this thesis are those of the author and do not reflect the official policy or position of the Department of Defense or the U.S. Government.

12a. DISTRIBUTION / AVAILABILITY STATEMENT
Approved for public release; distribution unlimited.

12b. DISTRIBUTION CODE

ABSTRACT *(maximum 200 words)*

The thermal control system of a spacecraft is designed to maintain all spacecraft components within their specified operating temperature limits throughout all phases of a spacecraft's mission. In order to verify and aid in such a design process, a thermal analysis of the system must be conducted. A thermal model of the spacecraft is used to simulate its behavior under given thermal environments and boundary conditions so that temperature predictions can be made.

The focus of this thesis is to develop and analyze thermal models of PANSAT which describe its thermal behavior while it is in orbit and also prior to its insertion in its orbit (while it is still in the shuttle). The results of these analyses will serve to help in the thermal design and performance of PANSAT. This thesis completes the thermal model prerequisites of the STS 95 space shuttle mission hitchhiker program for PANSAT. The emphasis of this thesis is to develop a model that will allow the prediction of the temperatures of all the electrical components including the temperature sensitive electrical components of PANSAT such as batteries over a complete orbit of the satellite.

14. SUBJECT TERMS
THERMAL ANALYSIS , SPACECRAFT THERMAL CONTROL

15. NUMBER OF PAGES
100

16. PRICE CODE

17. SECURITY CLASSIFICATION OF REPORT	18. SECURITY CLASSIFICATION OF THIS PAGE	19. SECURITY CLASSIFI- CATION OF ABSTRACT	20. LIMITATION OF ABSTRACT
Unclassified	Unclassified	Unclassified	UL

Approved for public release, distribution is unlimited

THERMAL ANALYSIS OF PANSAT

Travis R. Smith
Lieutenant, United States Navy
B. S., Virginia Polytechnic Institute and State University, 1990

Submitted in partial fulfillment of the

requirements for the degree of

MASTER OF SCIENCE IN ASTRONAUTICAL ENGINEERING

From the

NAVAL POSTGRADUATE SCHOOL

December 1997

Author: _____
Travis R. Smith

Approved by: _____
Oscar Biblarz, Thesis Advisor

_____
Ashok Gopinath, Co-Advisor

_____
Dan Sakoda, Co-Advisor

_____
Gerald Lindsey, Chairman
Department of Aeronautics and Astronautics

ABSTRACT

The thermal control system of a spacecraft is designed to maintain all spacecraft components within their specified operating temperature limits throughout all phases of a spacecraft's mission. In order to verify and aid in such a design process, a thermal analysis of the system must be conducted. A thermal model of the spacecraft is used to simulate its behavior under given thermal environments and boundary conditions so that temperature predictions can be made.

The focus of this thesis is to develop and analyze thermal models of PANSAT which describe its thermal behavior while it is in orbit and also prior to its insertion in its orbit (while it is still in the shuttle). The results of these analyses will serve to help in the thermal design and performance of PANSAT. This thesis completes the thermal model prerequisites of the STS 95 space shuttle mission hitchhiker program for PANSAT. The emphasis of this thesis is to develop a model that will allow the prediction of the temperatures of all the electrical components including the temperature sensitive electrical components of PANSAT such as batteries over a complete orbit of the satellite.

TABLE OF CONTENTS

I. INTRODUCTION

The objective of this thesis is to develop a model that simulates the transient and steady state thermal behavior of PANSAT (Petite Amateur Navy Satellite) while in flight/orbit under a given set of external thermal environments and boundary conditions. Once required model accuracy is attained, the model will be used to simulate different thermal environments in order to determine other design parameters, such as the amount and type of thermal insulation and shielding that is needed in order to maintain all spacecraft components within their specified operating temperature limits. The most temperature sensitive components are the batteries which have narrow temperature operating margins that must be maintained to ensure proper operation.

This thesis covers two distinct phases of the mission. The first phase is the time interval while PANSAT is in the Shuttle (as the Shuttle orbits the Earth), awaiting insertion into its orbit. The second period is the in-orbit phase of the mission when PANSAT has been inserted into its orbit and becomes fully operational. Each of the aforementioned periods will be modeled separately and analyzed under simulated thermal environments and boundary conditions. These models will be used for steady state analyses and transient analyses to predict real time thermal performance of the spacecraft systems and individual components.

A. PANSAT BACKGROUND

PANSAT is a small, direct sequence spread spectrum communications satellite being developed by the students, staff, and faculty at the Naval Postgraduate School (NPS). PANSAT serves as a hands-on educational project for officer students in numerous academic disciplines to gain knowledge in designing, building, testing, and operating small satellites. Additionally, PANSAT will serve as a proof of concept of low cost, spread spectrum, digital over-the horizon communications. Amateur radio operators will use PANSAT to store and forward communications once it is in orbit and ready for full operations. The Naval Postgraduate School mission control center will serve as the ground control center for the in-orbit phase of the mission.

PANSAT consists of a simple design in that it has no attitude control or propulsion system and weighs approximately 150 pounds. Hence, PANSAT is to be a tumbling spacecraft. PANSAT is currently manifested on the space shuttle mission (STS 95) which is scheduled to launch from Kennedy Space Center in Cape Canaveral, Florida in October 1998. PANSAT will be inserted into orbit by means of the space shuttle hitchhiker program ejection system. Silicon solar cells (manufactured by Spectralab Inc.) and nickel-cadmium battery cells (manufactured by Sanyo) will provide the power for PANSAT while it is in orbit. PANSAT will be in a low earth orbit with an inclination of approximately 28.5 degrees and an altitude of approximately 310 nautical miles (574 km). PANSAT has a two year design lifetime which is primarily a function the aerodynamic drag and radiation experienced by satellites at the low earth orbit altitudes [Ref. 3]. The aerodynamic drag, a non-conservative force, continuously extracts energy

from the orbit; thereby, causing the spacecraft to spiral into the earth's atmosphere and to subsequently burn up upon reentry [Ref. 3]. The high altitude of the STS-95 mission however, offers an orbit lifetime in excess of four years.

B. SPACECRAFT THERMAL CONTROL

The thermal control system of a spacecraft is designed to maintain all spacecraft components within their designed operating temperature limits throughout all mission phases. In order to complete the thermal design of a spacecraft, a thermal model of the spacecraft must be made which accurately depicts its thermal behavior under the given boundary and thermal environmental conditions. The focus of this thesis is to develop a thermal model that simulates the transient and steady state thermal behavior of PANSAT and to conduct thermal analyses to test the model and hence improve the thermal design and performance of PANSAT.

This thesis covers two periods. The first period is the time interval while PANSAT is in the Shuttle (as the shuttle orbits the Earth), awaiting insertion into its orbit. The second period is the time interval after PANSAT has been inserted into its orbit. Each of the aforementioned periods will be modeled separately and analyzed under simulated thermal environments .

1. Spacecraft Thermal Design

The thermal design of a spacecraft is affected by the power, attitude and control, communications, and structural subsystems [Ref. 6]. The interaction between these systems necessitate tradeoffs that significantly affect the design of the thermal control system. Normally, small, unmanned, low earth orbit satellites can be controlled passively

[Ref. 7]. Passive thermal control is preferred over active thermal control because of its simplicity, reliability, and lower costs. Active thermal control uses heaters, active mechanical, or active fluids devices in the design whereas passive thermal control use primarily thermal coatings, surface finishes, insulation, and equipment placement, and material selection in its design. Since PANSAT is in its advanced development stage, thermal coatings, surface finishes, and insulation will be considered for use at this point in the project. Normally, the thermal engineer interacts with the structural engineer, electrical power engineer, and attitude and control engineer in the early stages of the design in order to achieve optimum thermal design, system integration, and performance.

The first step in the thermal design process is to determine the component temperature limits, internal power dissipation, and environmental heat inputs incident on the exterior surfaces of the spacecraft [Ref. 7]. The thermal design of a spacecraft is an iterative process based on the successive thermal analyses of the thermal model under various boundary conditions and external thermal environments. Figure 1 illustrates the various inputs into the thermal design process and the outputs of the thermal analysis of a given model. The results of the analysis are subsequently used to improved the design and verify the tentative design. This iterative process continues until the desired optimization and system integration is achieved.

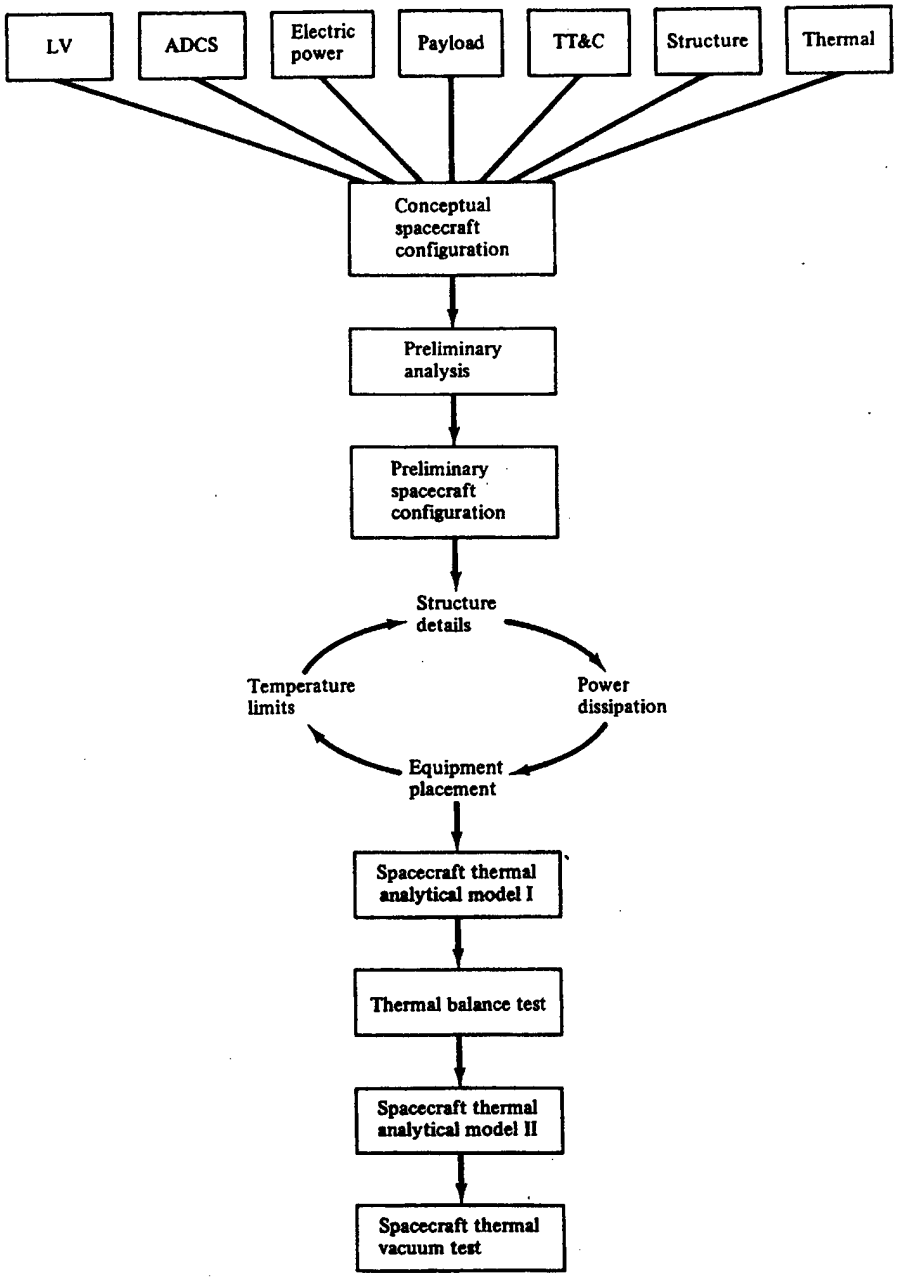

Figure 1. Thermal design process (Ref. 1)

II. THERMAL ENVIRONMENT

A. ORBIT ANALYSIS

As a member of the space shuttle hitchhiker program, PANSAT is considered to be a secondary payload; hence, it will have to accept the orbital elements of the primary space shuttle payload [Ref. 12]. PANSAT will be placed in a low-earth orbit of approximately 310 nautical miles with an inclination of approximately 28.5 degrees. It will be subject to various thermal environments depending on its location and attitude within the orbit. These inputs include ultraviolet solar radiation, ultraviolet earth reflected solar radiation, and infrared earth emitted radiation. The rate at which the spacecraft and the space environment exchange heat is primarily dependent upon the temperature of the two bodies. Since the spacecraft thermal environment heat varies with spacecraft altitude, spacecraft attitude, and spacecraft position in the orbit. The heat fluxes incident upon PANSAT vary also. The classical orbital elements, explained in Table 2.1 and shown in Figure 2, completely describe the orbit of any object.

ORBITAL ELEMENT	SYMBOL	DESCRIPTION
Semi-major axis	a	Size of the ellipse
Inclination	I	Angle between earth's equatorial plane and the satellite orbital plane
Eccentricity	e	Shape of the ellipse
Right ascension of the ascending node	Ω	Angle from vernal equinox to ascending node
Argument of perigee	ω	Angle between the ascending node and the point of periapsis, measured in satellites orbital plane
True anomaly	υ	Angle from the point of periapsis to satellite's position

Table 2.1 Classical orbital elements

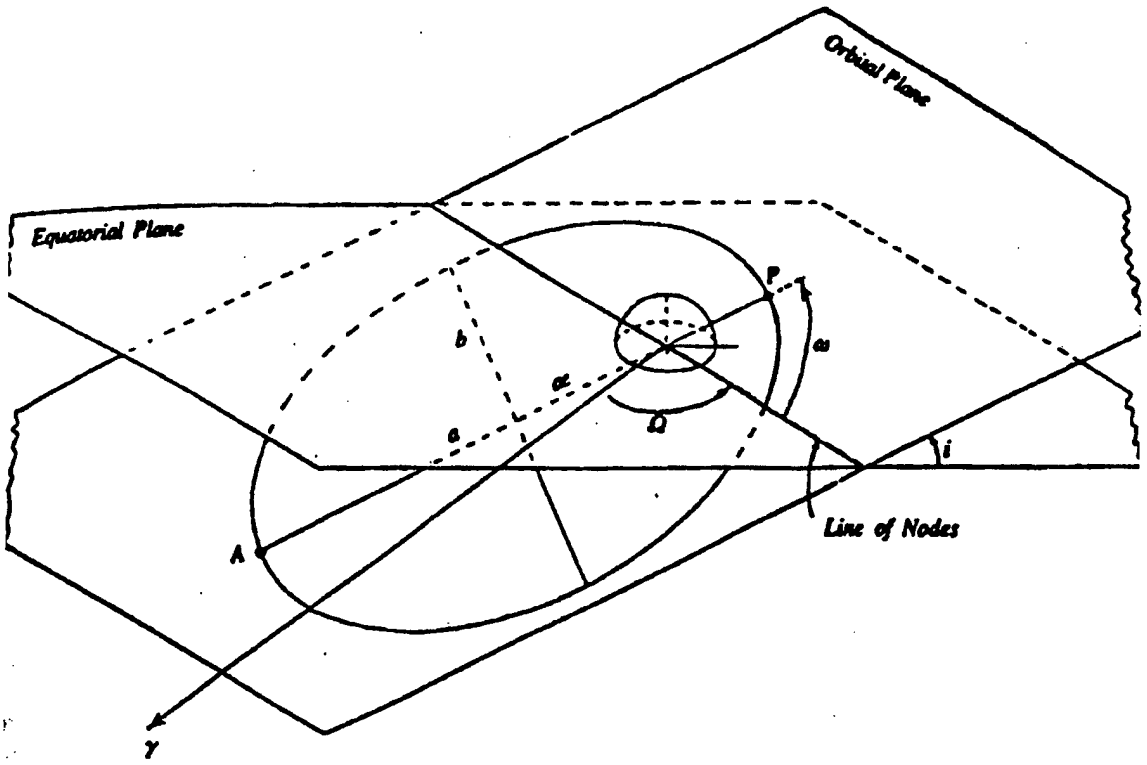

Figure 2. Classical orbital elements

These classical orbital elements determine the duration of the sunlight and eclipse portions of the orbit. The duration of the sunlight portion of the orbit and the eclipse portion of the orbit have a significant impact on systems operations, the electrical power system and consequently the thermal control system. Low earth orbit spacecraft have shorter and more frequent eclipse periods than geosynchronous earth orbit spacecraft which result in higher discharge and recharges rates for the batteries. The excess heat generated by the cyclic charge and discharge creates more heat for the thermal control system to manage.

Figure 3 shows the period, minimum and maximum eclipse time for circular orbits at various inclinations. For PANSAT'S orbit (i=28.5, altitude=310 nautical miles, e=0) the period is approximately 95 minutes with an maximum eclipse duration of approximately 36 minutes [Ref. 10].

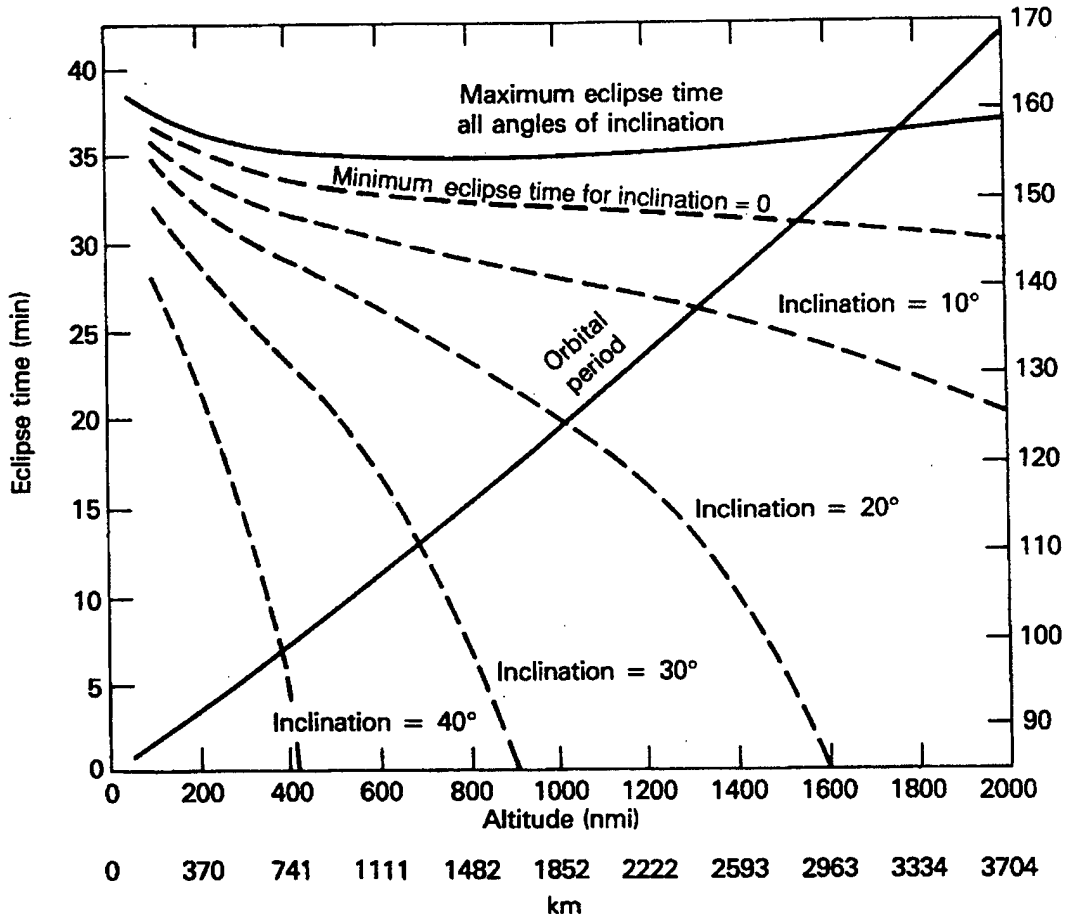

Figure 3. Orbital period, maximum and minimum eclipse time for circular orbits (Ref. 10)

The minimum eclipse duration increases as the inclination of the spacecraft decreases for a given altitude. In addition, the period increases or decreases with a corresponding change in altitude [Ref.10].

B. EXTERNAL THERMAL ENVIRONMENT

Figure 4 depicts the various heat sources and sinks that a spacecraft in low earth orbit experiences [Ref. 12]. The heat sources are direct solar radiation, reflected solar radiation from the Earth, emitted infrared radiation from the earth, and internal heat dissipation from the internal components of the spacecraft. The majority of the Solar and reflected radiation is in the ultraviolet region [Ref. 6]. The spacecraft exchanges heat with space, a heat sink, via radiation. The solar intensity varies approximately 3.5% due to the Earth's elliptical orbit [Ref. 6]. The environmental heat inputs are defined using solar vector angles usually referred to as the beta angles. A beta angle of 23.5 degree is equivalent to a solar incidence angle of zero upon the spacecraft which is the worst case angle.

The attitude of a spacecraft normally has a direct impact on most spacecraft; however, because PANSAT has no attitude control system, the spacecraft will tumble throughout its orbit. The most likely orientations will be investigated in this thesis. The non-tumbling orientation would have a tendency to set up thermal gradients because of the prolonged exposure of a particular surface to a particular environment.

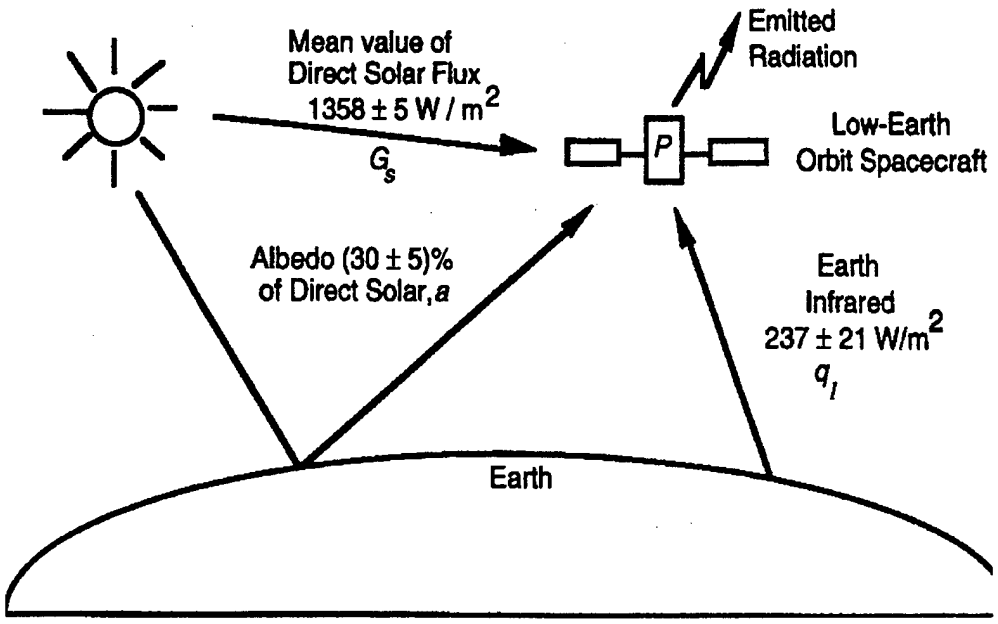

Figure 4. Spacecraft thermal environment in LEO (Ref. 14)

III. SPACE CRAFT CONFIGURATION AND DESIGN

A PHYSICAL DESCRIPTION OF PANSAT

A schematic of PANSAT is shown in Figure 5. PANSAT is a 26 sided polyhedron and has a highly symmetric structure. This configuration was chosen because PANSAT has no attitude control or propulsion system. PANSAT is divided into three modular sections: the upper deck, the mid-deck and the lower deck. These sections are shown in more detail in Figures 6, 7, and 8. These sections consist of a top panel, a bottom panel, four upper deck and four lower deck panels, and eight mid-deck panels. The upper and lower sections have four triangular plates with the antennae mounted on the plates of the upper section. These antenna subassembly plates have testing ports and lifting eyes for PANSAT and have bare surfaces. The remaining panels are each covered with a layer of silicon solar cells manufactured by Spectralab Inc., and serve as a solar collector. These cells (model K6700A) have a mass of 55 mg/cm^2 and an efficiency of 14.6% (based on the manufacturer's data sheet). The launch vehicle interface (LVI) connects PANSAT to the base of the (GAS) canister via a base plate or bottom plate which is in turn connected to the space shuttle.

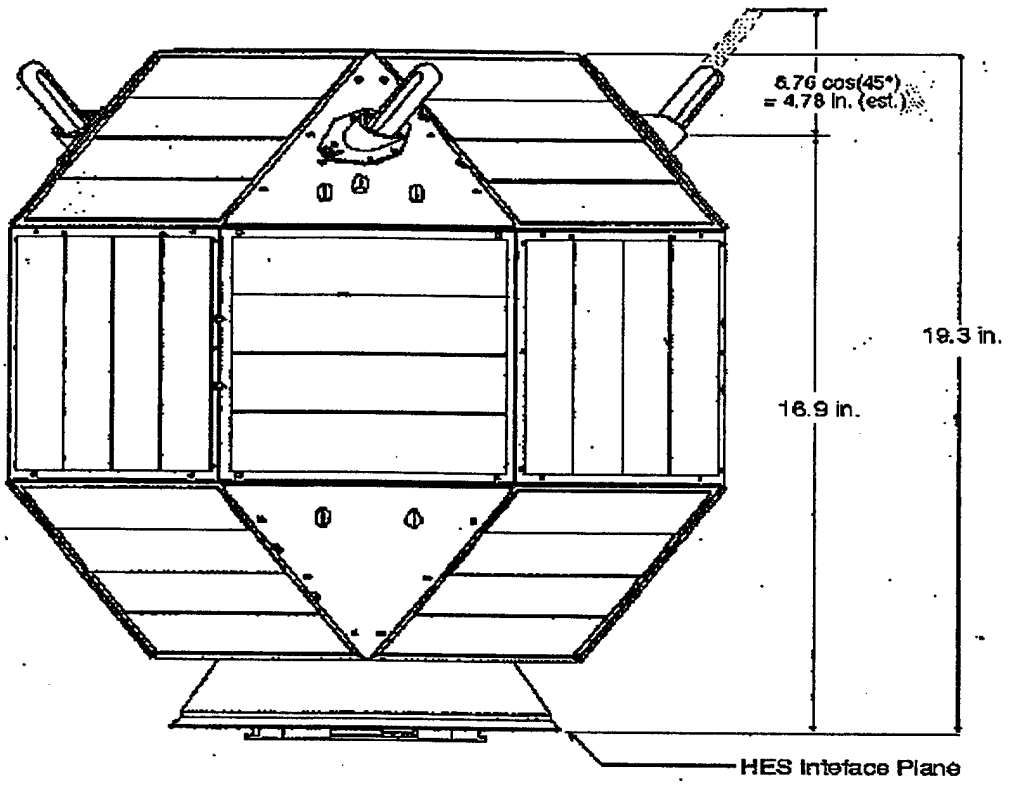

Figure 5. PANSAT exterior structure with the launch vehicle interface

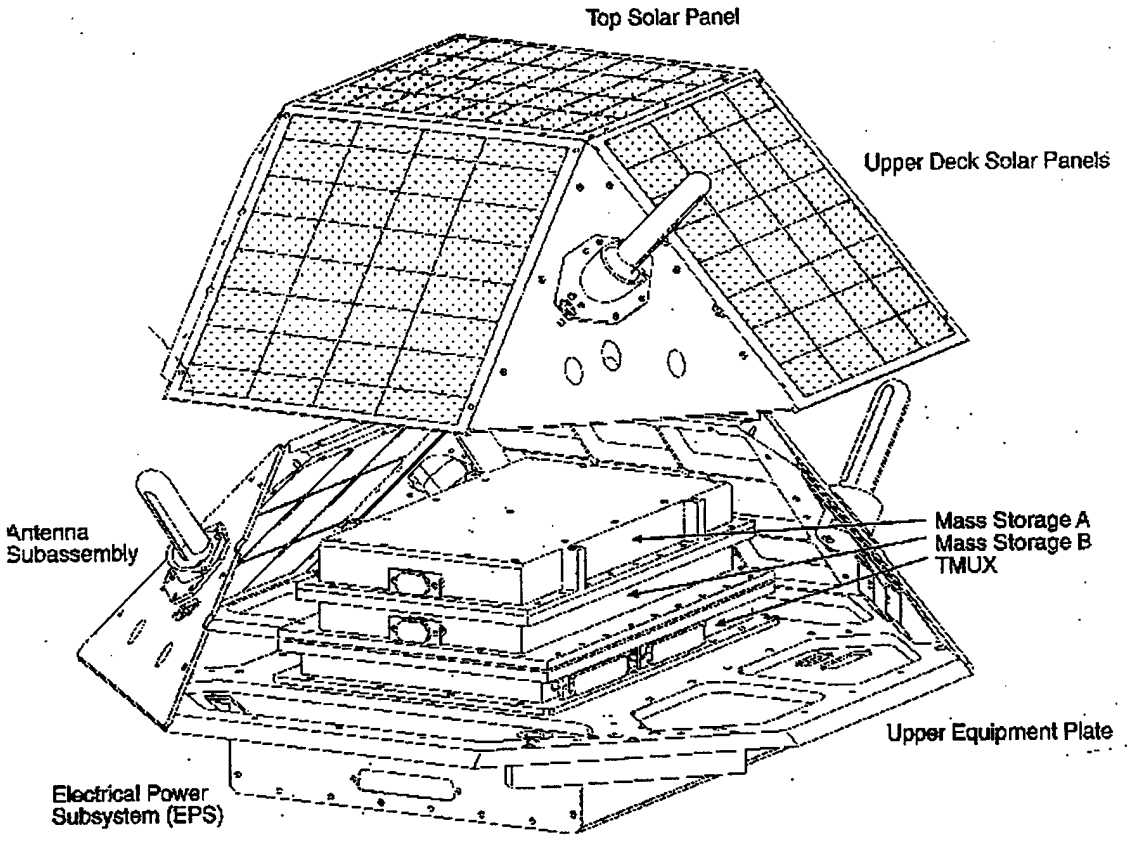

Figure 6. Upper deck configuration

The configuration of the upper deck of PANSAT is shown in Figure 6. The upper module contains the mass storage containers A and B, the upper equipment plate, four triangular antenna subassembly plates, a top panel and four upper deck panels, and a temperature sensor multiplexer (TMUX). The mass storage compartments are assumed to have perfect contact with each other and the TMUX. The TMUX is also assumed to have perfect contact with the upper equipment plate. The electrical power system (EPS) is not part of the upper section but is mounted on the bottom of the upper equipment plate with fasteners. All panels except the antenna subassembly panels are covered with silicon solar cells on the outside.

The top panel is a square whose side is 7.125 in. in length and has a thickness of 0.25 in. The upper equipment plate is an octagon whose sides are also 7.125 inches in length. Each side has a 125-135 degree taper with a thickness of 0.25 inches. The top

panel is attached to the other four upper deck panels via six 4-40 screws. The four upper deck panels are 7.125 in. x 8.250 in. Each panel has a 35 degree taper.

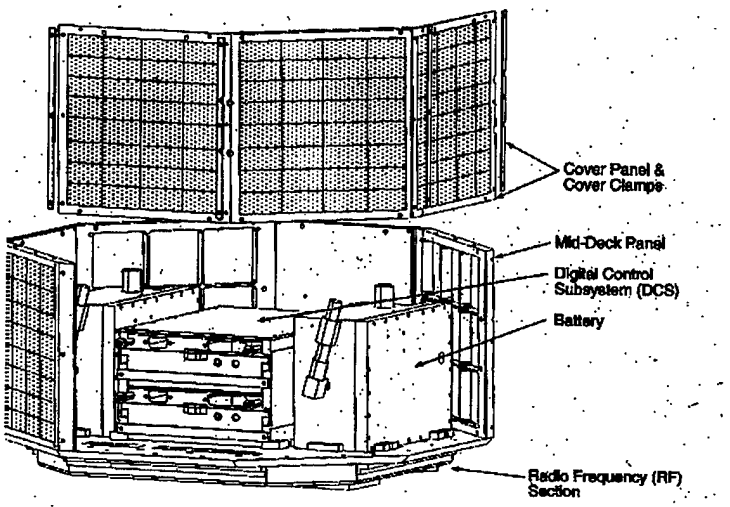

Figure 7. PANSAT mid-deck configuration

The mid-deck section of PANSAT (shown in Figure 7) consists of eight deck panels, the electrical power system (EPS), battery compartments A and B, the digital control system (DCS), and the lower equipment plate (LEP). The radio frequency section is mounted on the bottom of the lower equipment plate although it is not part of the mid-deck section. There is a 0.5 in. gap between the DCS and the battery compartments. The DCS and the battery compartments are mounted on the LEP with fasteners. The exterior of all eight panels is covered with silicon solar cells. These panels are 7.125 in. x 7.125 in. on a side, and 0.063 inches thick. These panels exchange heat externally by radiation with the walls of the GAS canister, while they primarily exchange most of their heat by conduction with the internal components of PANSAT.

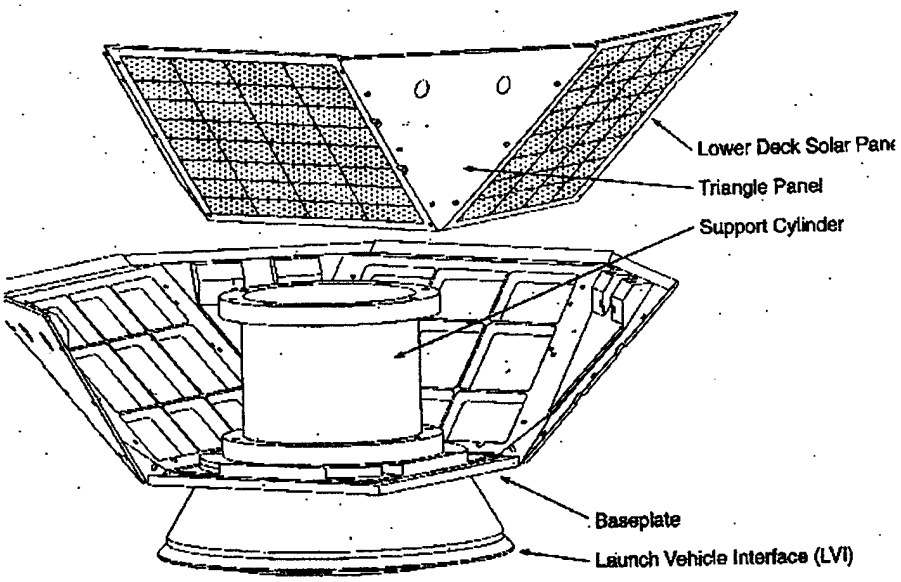

Figure 8. PANSAT lower deck configuration

The lower module of PANSAT (shown in Figure 8) contains the radio frequency section, the support cylinder, the base plate or bottom plate, four lower deck panels and four triangular plates. The support cylinder made of aluminum is hollow and attaches directly to the lower equipment plate (LEP) and the base plate of PANSAT. The LVI attaches to the base plate and connects PANSAT to the base of the GAS canister. In this model, the LVI is lumped together with the base of the GAS canister and together assumed to be thermally massive.

IV. THERMAL MODELING

A. HEAT TRANSFER

1. Conduction

Conduction heat transfer occurs between two solid or fluid objects in physical contact with each other under the influence of a temperature gradient [Ref. 1]. Heat transfer occurs across the medium. Conduction is simply the transfer of kinetic energy from more energetic particles to the less energetic particles [Ref. 4] . The basic law of one dimensional conduction is governed by the Fourier's equation.

$$Q = -kA\frac{dT}{dX} \qquad [4.1]$$

Where,

Q= the rate of heat conduction along the x axis ,W

k= thermal conductivity, a physical property of the material , W/m-K

A= cross sectional area of the path normal to the x axis ,m^2

$\frac{dT}{dX}$ = temperature gradient along the conduction path, $\frac{K}{m}$

The thermal conductivity (k) varies with temperature; but, may be assumed to be constant over the a given temperature range [Ref. 6]. The conduction heat transfer is analogous to the Ohm's law for electricity [Ref. 1]. The heat flow ,Q, represents the current. The temperature gradient, dT, represents the voltage and kA/dx represents the conductance which is the reciprocal of the thermal resistance [Ref. 1]. The conductances,

the reciprocal of the thermal resistances, account for the heat transfer between nodes as shown in Equation 4.2 and Figure 9.

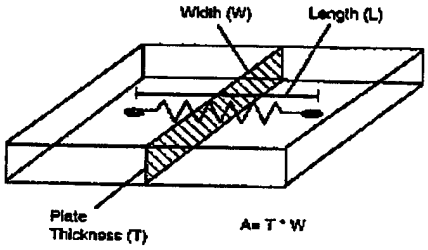

Figure 9. Geometry to calculate linear conductances

$$C = \frac{kA}{L} \qquad [4.2]$$

where,

C = Linear conductance (W/K)
k = Thermal conductivity (W/m-K)
A = normal cross sectional area between nodes(m^2)
L =distance between nodes(center to center) (m)

Contact between to surfaces are rarely perfect and the pressure applied to any component is rarely uniformly distributed. Thus, there is a contact resistance at the surface interfaces of the two objects. This contact resistance plays an important role when boxes are mounted to surfaces within the spacecraft. (i.e., DCS, battery compartments, EPS, and RF COMMS). The contact conductance varies with the hardness of the material, surface finishes, surface contact area, and the pressure applied [Ref. 6].

Gap filler material is used in order to fill the void due to surface roughness and increase thermal conductivity [Ref. 6].

2. Radiation

Radiation is electromagnetic energy that is emitted from all bodies whose temperatures are above absolute zero [Ref. 7]. Radiative heat transfer is defined by the Stefan-Boltzmann law and varies as the fourth power of the temperature [Ref. 7]. Hence, at lower temperatures, larger areas are required to reject a given amount of heat. Radiative heat transfer does not required objects to be in physical contact. Radiation can take place in a vacuum and is a function of temperature of emitting and receiving bodies (at least one temperature must be above absolute zero) , the surface properties of the material of the bodies, the intervening medium, and the relative geometry. The total radiation incident upon a spacecraft is either absorbed, reflected, or transmitted [Ref 7]. The radiation that is absorbed must be managed by the thermal control system. Equation 4.3 describes radiation heat transfer.

$$q = \varepsilon\sigma T^4 \qquad [4.3]$$

Where,

q= total energy radiated per unit area

ε = emissivity

σ = Stefan Boltzmann Constant

T= absolute Temperature in Kelvin

The relative geometry of the surfaces plays a major role in radiation heat transfer. This geometry is characterized by a view factor which relates the fraction of energy emitted from one surface that is intercepted by another surface [Ref. 4]. Figure 10 shows the radiation heat exchange between two surfaces and equations 4.4 and 4.5 depict the view factor of surface 1 with respect to surface 2 [Ref. 4].

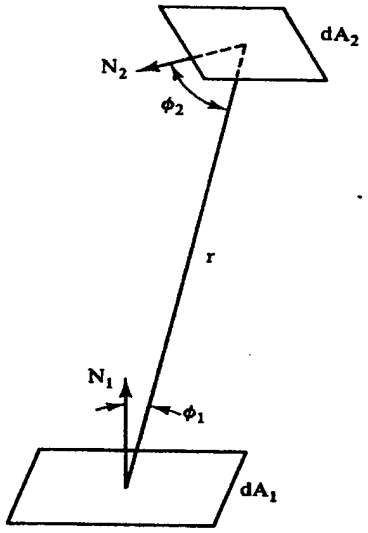

Figure 10. View factor associated with the radiation heat exchange between two surfaces (Ref. 1)

$$F_{12} = \frac{1}{A_1} \int_{A_1} \int_{A_2} \frac{\mathrm{dA}_1 \cos\phi_1 \; dA_2 \cos\phi_2}{\pi r^2} \qquad [4.4]$$

Where,

F_{12}= view factor from surface 1 to surface 2

A_1 = area of surface 1 (m^2)

A_2 = area of surface 2 (m^2)

ϕ_1= angle between normal and surface 1

ϕ_2= angle between normal and surface 2

The amount of radiation emitted from surface 1 that is incident on surface 2 is given by the following relationship.

$$Q_{12} = A_1 F_{12} \sigma (T_1^4 - T_2^4) \qquad [4.5]$$

where,

Q_{12}= the net heat exchange between two diffuse gray surfaces 1and 2 (W)

A_1 = area of surface 1 (m^2)

σ = Stefan Boltzmann constant (W/m^2K^4)

T_1 = temperature of the surface (K)

T_2 = temperature of the surface (K)

F_{12}= view factor from surface 1 to surface 2

3. Convection

Convection is heat transfer between a flowing liquid and a solid interface [Ref. 13]. Convection plays a minor role in low-Earth orbit, unmanned spacecraft and is not discussed in this thesis [Ref. 13].

B. LUMPED PARAMETER MODELING

1. Thermal Nodes

The thermal behavior of satellites is completely described by the thermal capacities (nodes), conductors, and radiative couplings which form the analytical model [Ref. 7]. Although the surface properties of the nodes degrade over an extended period of time, the optical properties (absorptivity and emissivity) change minimally for an 2-4 year design lifetime of PANSAT. For longer in-orbit phases, and greater altitudes, the absorptivity increases and the infrared emissivity remains relatively constant. Therefore, end of life (EOL) optical properties are used in thermal control system design.

The size and selection of nodes are chosen so that they are isothermal. A material with a high thermal conductivity such as aluminum can be considered isothermal. The nodes contain all the mass, geometry, and optical properties.

C. ASSUMPTIONS

1. PANSAT In The GAS Canister

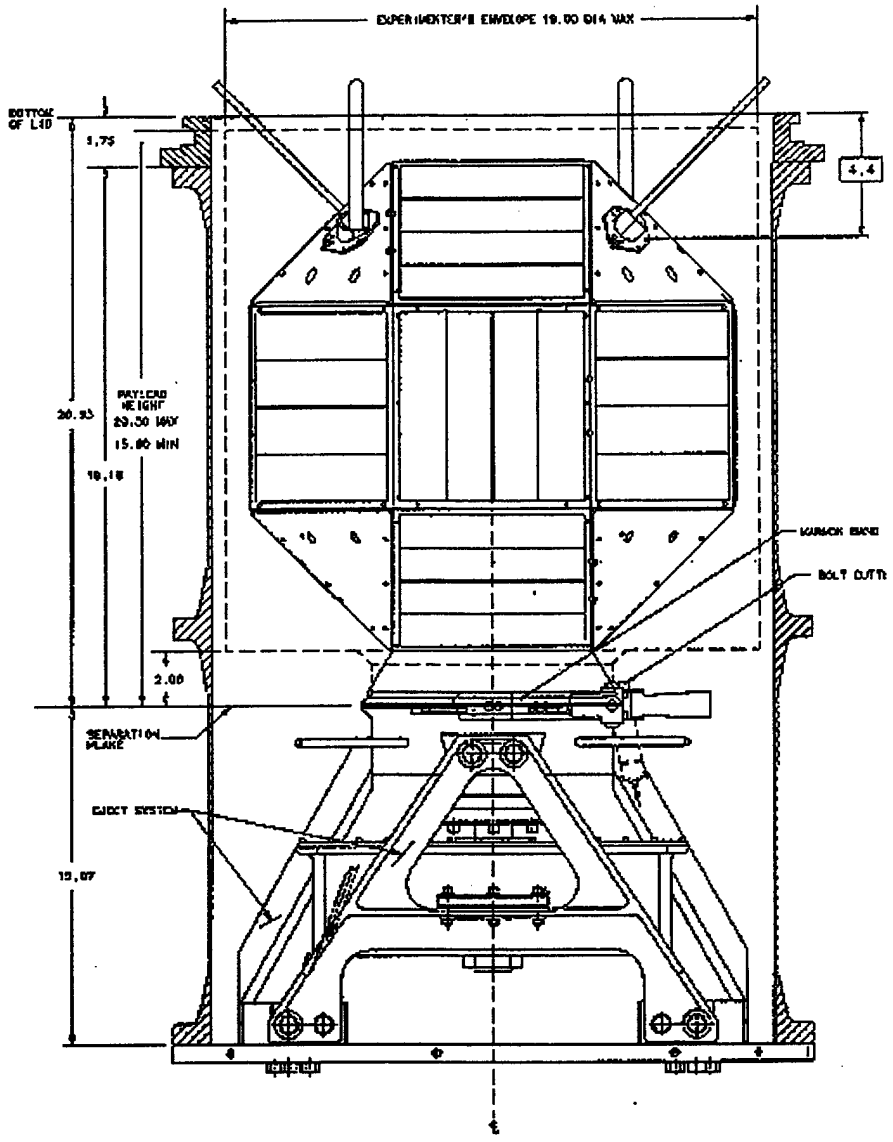

Figure 11. PANSAT in the gas canister

The thermal model is based on a lumped nodal analysis of the various key components of this configuration [Ref. 2]. In all, the physical setup comprising PANSAT and the GAS canister have been broken down into 12 nodes, with each node representing a region which may be treated as isothermal. In the model of Figure 11, the nodes are

allowed to exchange heat with one another by conduction depending on thermal contact, and/or by radiation depending on the view factor geometry [Ref.4]. A schematic of the nodal network is shown in Figure 12, and the details of each node are provided in Appendices A and B.

The major assumptions in setting up the model are the following:

- The solar constant (solar radiation flux) is taken to be invariant at 1353 W/m^2 over the entire orbit [Ref. 1].
- The top, mid-deck and bottom sections and enclosures, each make up an isothermal node and have uniform radiosity and irradiation characteristics [Ref. 3].
- All surfaces exhibit opaque, diffuse, gray surface behavior.
- Each node is isothermal with all the material and thermal properties of the region it represents being lumped into the node.
- The mass of the base of the GAS canister coupled with the shuttle is sufficiently large such that its temperature does not vary over the course of this analysis.
- Only the top section of PANSAT receives direct solar radiation in this model. The mid-deck and lower sections are not exposed to space while PANSAT is in the GAS canister due to the close proximity of their walls.
- No single section of PANSAT sees the entire inner surface of the can - different sections see different portions of the GAS canister depending on their location and orientation.
- The four strip heaters located in the lower part of the GAS canister see only the lower deck section of PANSAT, and each provides equal heat distribution to PANSAT.
- All the electronic boxes and components inside PANSAT which are fastened or bolted to one another are in perfect thermal contact.
- All of the triangular antenna subassembly panels are also taken to be covered with solar cells.
- The mass of the solar cells themselves are neglected in the calculations of the nodal masses.

- The GAS canister can receive solar radiation in an unobstructed manner.
- A representative temperature of 250 K is assumed as the initial temperature in this analysis. Such a choice however is not restrictive in the interpretation of the results as discussed later in Section 9.
- All satellite materials are isotropic and their properties are constant over the temperature range of interest.

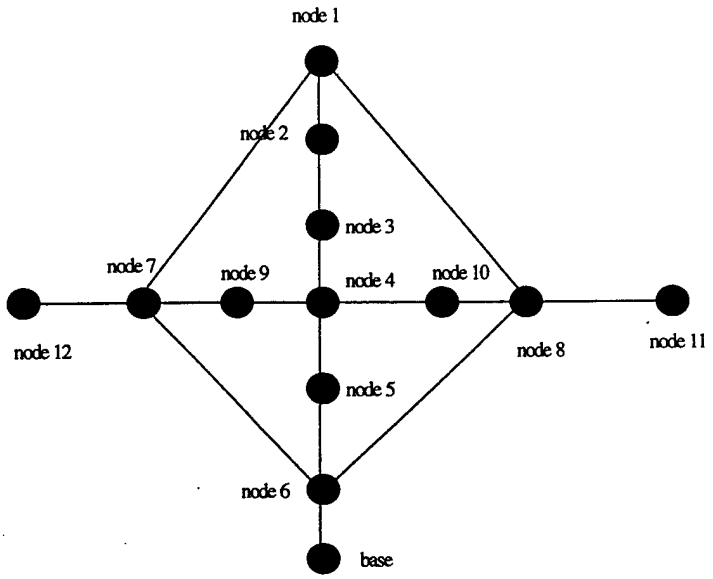

Figure 12. The thermal network model (in the canister)

2. PANSAT in Orbit

PANSAT is in its orbit and fully operational in this model. The LVI is still attached to the spacecraft as shown in Figure 5.

The major assumptions concerning this model are:

- The top, mid-deck and bottom sections and enclosures, each make up an isothermal node and have uniform radiosity and irradiation characteristics [Ref. 3].

- All surfaces exhibit opaque, diffuse, gray surface behavior.

- Each node is isothermal with all the material and thermal properties of the region it represents being lumped into the node.

- All the electronic boxes and components inside PANSAT which are fastened or bolted to one another are in perfect thermal contact.

- All of the triangular antenna subassembly panels are also taken to be covered with solar cells.

- The mass of the solar cells themselves are neglected in the calculations of the nodal masses.

- A representative temperature of 250 K is assumed as the initial temperature in this analysis.

- All satellite materials are isotropic and their properties are constant over the temperature range of interest.

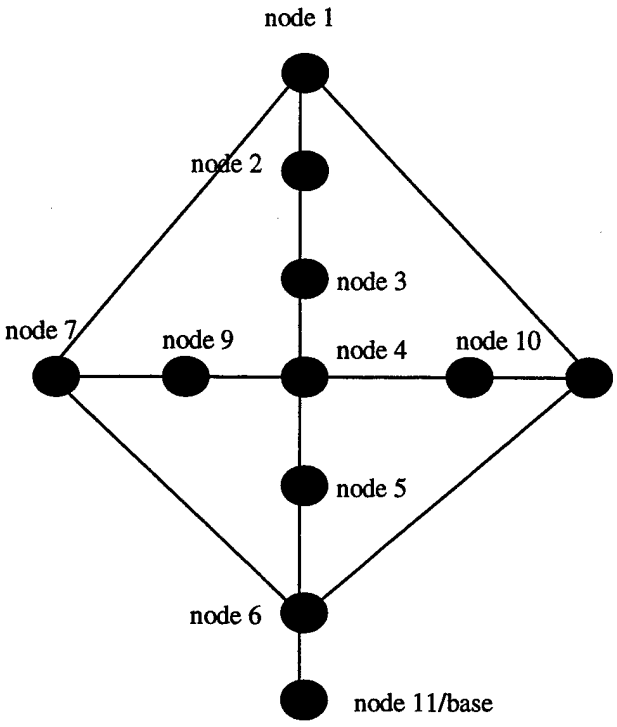

Figure 13. The thermal network model (in orbit)

D. BOUNDARY CONDITIONS

1. PANSAT in the GAS Canister

Nodes 2,3,4,5,9, and 10 are the interior nodes and do not exchange heat directly with the external ambient. Nodes 1,6,7,8,11,12 on the other hand have exterior surfaces that can exchange heat with the external thermal environment. Of these, only nodes 1, 11 and 12 representing the top panels of PANSAT, and the sides of the GAS canister respectively, receive solar radiation. The base of the GAS canister serves effectively as a heat sink which tends to transfer all the heat from PANSAT into the Space Shuttle. The exterior surface of the GAS canister is covered with thermal beta cloth. All of the kapton strip heaters are taken to be either on, or off, at a particular instant in time. The battery compartments (nodes 9 and 10), the EPS (node 3), the RF communications box (node5),

and the DCS (node 4) are not powered during these storage conditions and produce no heat while PANSAT is in the GAS canister.

2. PANSAT in Orbit

The boundary conditions in this model are similar to the previous model with following exceptions. The GAS canister (nodes 11 and 12) is absent. The launch vehicle interface (LVI) is node 11 in this model. The batteries, DCS, RF COMMS, and EPS are powered during this phase. The interior nodes are the same as in the previous phase. Nodes 1,7,8,9,6, and 11 are the exterior nodes and can exchange heat with the external thermal environment.

Equation 4.2 was used to calculate the conduction heat transfer conductance between the various nodes in thermal contact [Ref. 1]. This value of conductance is based on the geometry of the section and the material used. It is not temperature dependent since material properties are assumed to be constant. The contact area is assumed uniform with an even pressure distribution. These values for the conductances are tabulated and listed in Appendix A. The area is the common cross sectional area of the two surfaces in contact. The area is the smaller of the two areas if the surfaces are of unequal sizes. The length, L, is the distance between the nodes normal to this cross sectional area as shown in Figure 10.

Equation 4.4 refers to heat transfer by radiation and is dependent upon the current temperature of the nodes in question [Ref.1]. In the model, the radiation conductance value is calculated for each time interval to get the most accurate value for the conductance at that instant in time. Thus the value of the radiation conductances are modified in the time integration process as the temperatures approach their steady state values.

Equations 4.3 and 4.5 are used to establish the heat balance at each node [Ref. 1]. The net heat exchange at each node is determined, and is set equal to zero for a steady state solution. The transient solution, however, is dependent upon the thermal capacitance of each node and the net energy in-flow into the node.

V. METHODOLOGY

A. PROGRAM CODE

1. PANSAT in the GAS Canister

The models described above and the associated time integration procedure were implemented with the help of Matlab (the source code listing for which has been provided in Appendix D). The time integration procedure is carried out for each of the twelve individual nodes (base excluded) simultaneously in a coupled manner to obtain the transient values for each nodal temperature, and to study their evolution to their respective steady state values.

Using the model and assumptions described in Section 4, PANSAT has been divided into ten different nodes (nodes 1-10) while the GAS canister was divided into three nodes (11,12 and the base). See Appendices A and B for the composition and description of each node. The twelve nodes, not including the base node, give twelve nodal energy balance equations at a given instant in time. These twelve equations form a system of 12 coupled nonlinear (due to the radiation terms) ordinary differential equations that are solved simultaneously using the "ode45" differential equation solver in Matlab. As an initial condition, all nodal temperatures are assumed to start with the same value as in the case when the Shuttle bay doors are just opened. In this analysis, the initial nodal temperature was taken to be 250 K. However, it is only the base that is assumed to have a large enough thermal mass so as to remain essentially constant at this temperature throughout the simulation. The output of this program is a time vector and a temperature matrix which provides a temperature for each node at each instant in time in the integrating process. For more details of the program implementation, reference may be made to the listing of the Matlab function which is provided in Appendix D. The user inputs the initial start time (to), the final stop time (tf) in seconds, and the uniform initial temperature in a 12 X 1 initial condition vector (T0) in this Matlab function.

the "ode45" integration procedure is carried out with the help of this function to integrate the coupled equations in time.

Several representative cases were run to see the trends in nodal temperatures for different values of the solar incidence angle and the strip heater power input. The following cases were tried:

CASE #	SOLAR INCIDENCE ANGLE (DEGREES)	HEATER POWER (W)
1A	0	0
1B	0	88
2A	45	0
2B	45	88
3A	90	0
3B	90	88

Table 4.1. Test cases used for analysis (in the canister)

It may be recalled that each heater has a 22 W capacity. All the heaters were either on or off during the simulation. Each provided an even distribution of heat to the lower deck of PANSAT. The other components of PANSAT are assumed to have no power dissipation in these cases.

2. PANSAT in orbit

The same methodology is the same as was used above in part 1, except that there are eleven nodes, and hence eleven nodal equations. The base (node 11) temperature is not fixed to the base temperature as in the previous case and are allowed to evolve

naturally. Table 4.2 presents the cases that were viewed for the in-orbit case. The orientations are shown in Figure 14 below and are assumed to be constant over the entire orbit.

CASE #	SOLAR FLUX	ROTATION RATE	HEAT DISSIPATION	ORIENTATION
	W/m^2	Deg/sec	W	anti-earth
4A	1399	0	21	node 1
4B	1309	4	0	node 1
5A	1399	0	21	node 7
5B	1309	4	0	node 7

Table 4.2. Test cases used for analysis (in orbit)

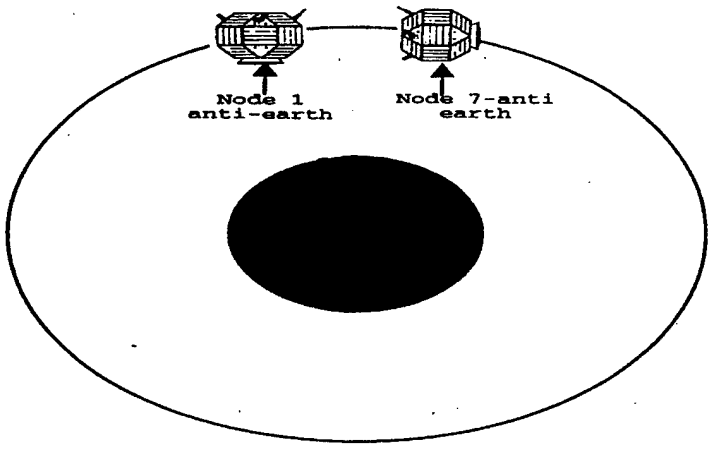

Figure 14. Orientations of PANSAT

VI. RESULTS AND DISCUSSION

The results and discussion are presented below for the two cases of PANSAT (A) the gas canister and (B) in orbit. The time integration is only for 90 minutes because the period of the orbit is approximately 90 minutes based on the scheduled altitude of 574 km as shown in Figure 3. The altitude of the mission could change. However, the space shuttle has maximum altitude constraints. Furthermore, PANSAT has no propulsion to change its altitude once in orbit. Hence; PANSAT should have a period of approximately 90 minutes with an eclipse time of approximately 30 minutes throughout its lifetime.

A typical low earth orbit has a period of approximately 90 minutes and an eclipse period of approximately 30 minutes. The period increases with an increase in altitude. Conversely, the eclipse time decreases as the altitude increases.

A. PANSAT IN THE GAS CANISTER

The results from the six cases tabulated above are depicted in the following pages in the form of temperature-time plots showing their approach to steady state conditions. The first graph in each set shows the variation of the temperature of the external nodes (1,6,7,8,11,12) with time. The second graph of each set is the temperature of the internal nodes (2,3,4,5,9,10) as it varies with time.

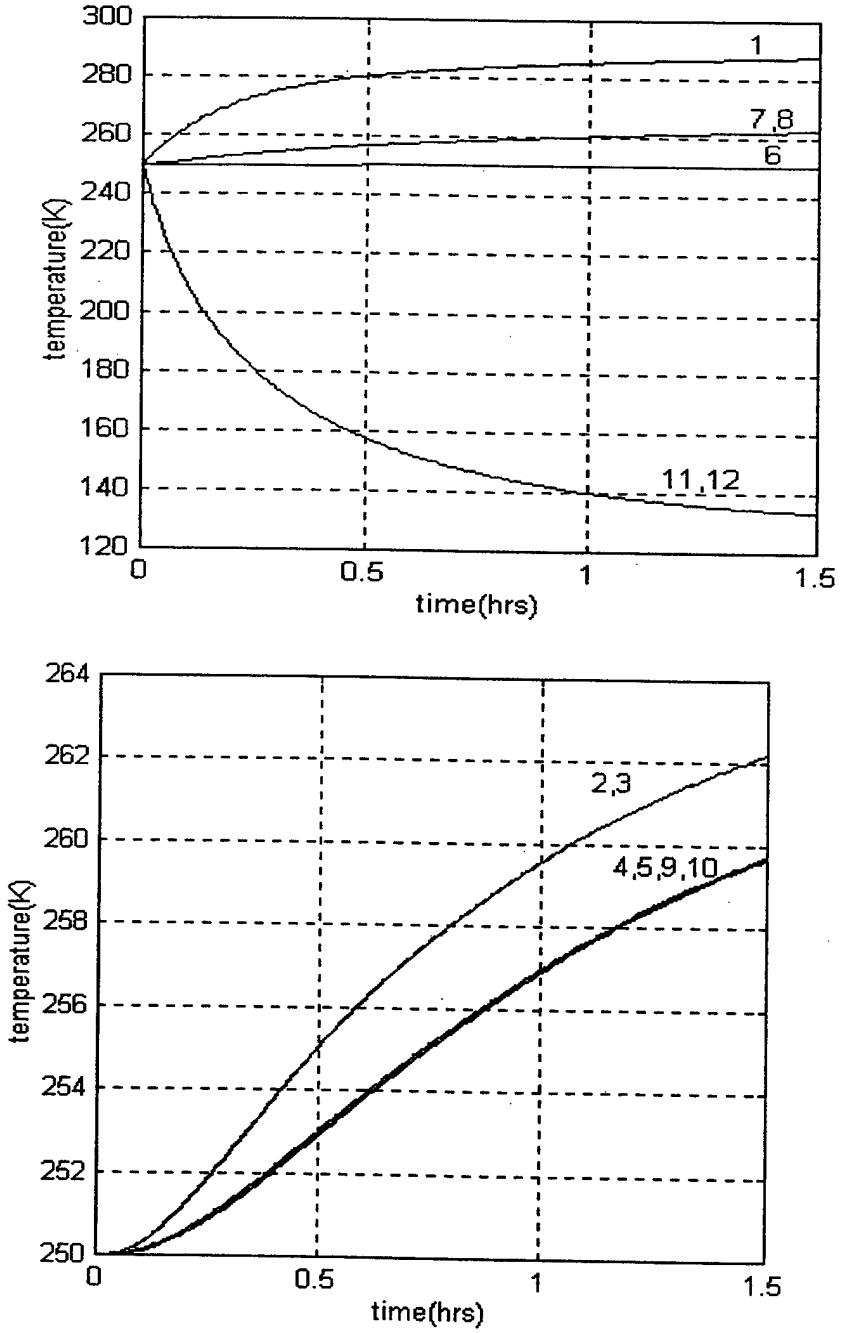

Figure 15. Nodal temperatures vs time. case 1A.

Figure 15 shows the temperature variation for normal solar incidence (zero angle) with the heaters off. Note that nodes 11 and 12 (the GAS canister walls) experience the

lowest temperatures since they do not receive any sunlight in this orientation, and are exposed to cold black space. The highest temperature is felt at node 1 because it receives direct sunlight at normal incidence. The temperature of node 6 does not change appreciably. There are several reasons for this behavior: node 6 has several conduction paths to lose heat (via nodes 7,8,11,12,base). In particular the conduction between node 6 and the base of the GAS canister is very large due to the large thermal mass of the base and its role as an effective heat sink. Thus there is a short circuit effect between node 6 and the base which plays a dominant role in the steady state and transient analyses. Furthermore, the internal nodes (2,3,4,5,9,10) are bounded by the temperature of node 1 and node 6.

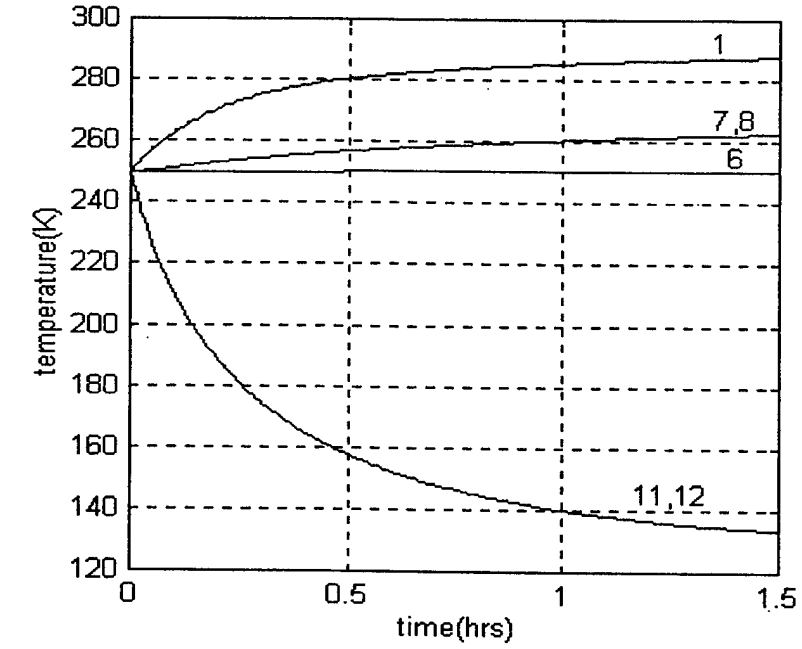

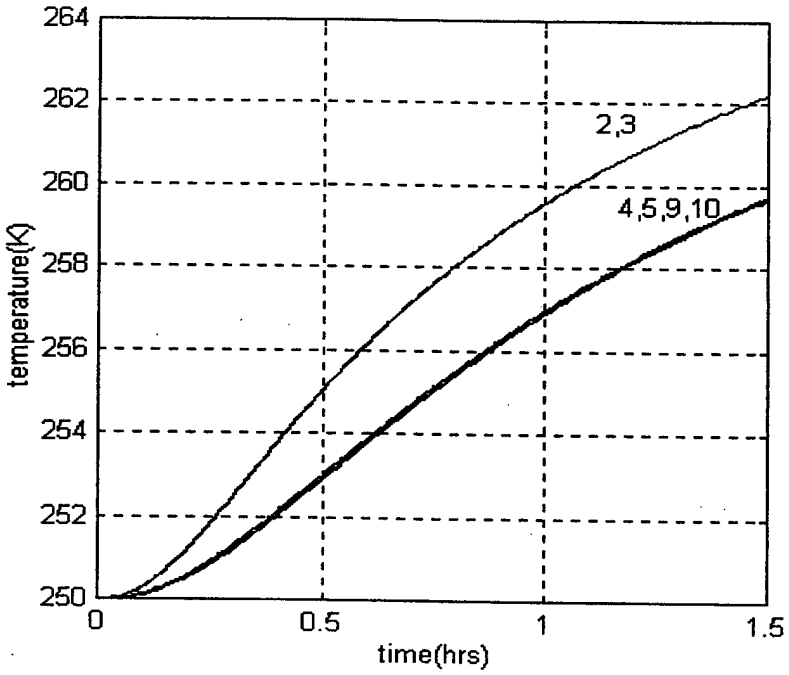

Figure 16. Nodal temperatures vs time. case 1B

Figure 16 is the same case as in Figure 15 except that the heaters are turned on. Recall that the combined power of the heaters is 88 W. This power has a negligible heating effect on node 6 (and PANSAT) primarily due to the short-circuit effect noted earlier by which heat transferred to node 6 is more easily conducted away through the base, rather than being transferred into PANSAT.

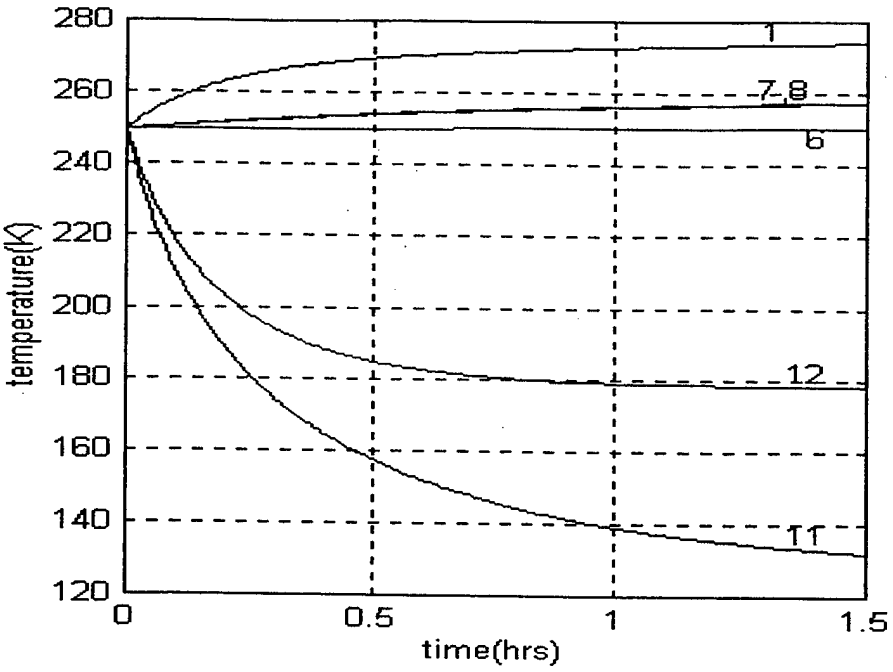

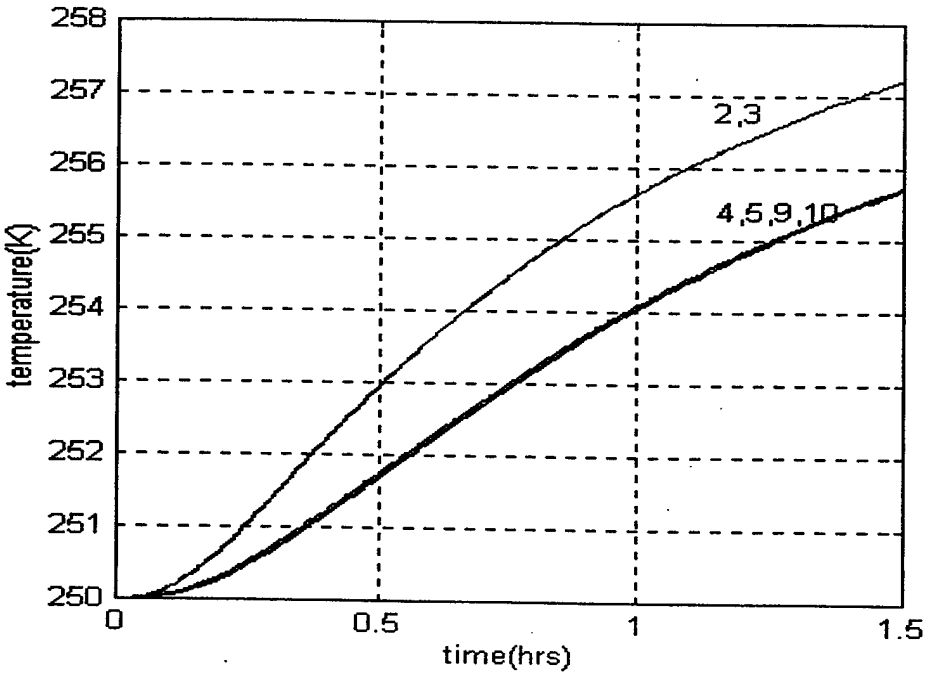

Figure 17. Nodal temperatures vs time. case 2A

Figure 17 depicts the temperature variation with time for a solar incidence angle of 45 degrees with the heaters off. The net effect of this new configuration is that the heat input to node 1 (top panels) is reduced, while the heat input to node 11 (one half of the GAS canister) is increased. As a result the temperature of node 1 is less than that in the normal incidence case . The temperature of node 11 is higher than that of node 12 since it receives direct sunlight whereas node 12 does not. Also, the temperature of node 7 is slightly greater than node 8. In contrast, note that in Figures 12 and 13, nodes 11 and 12 were at roughly the same temperature. Once again, the temperature of node 6 remains relatively constant over the time period it takes to reach steady state.

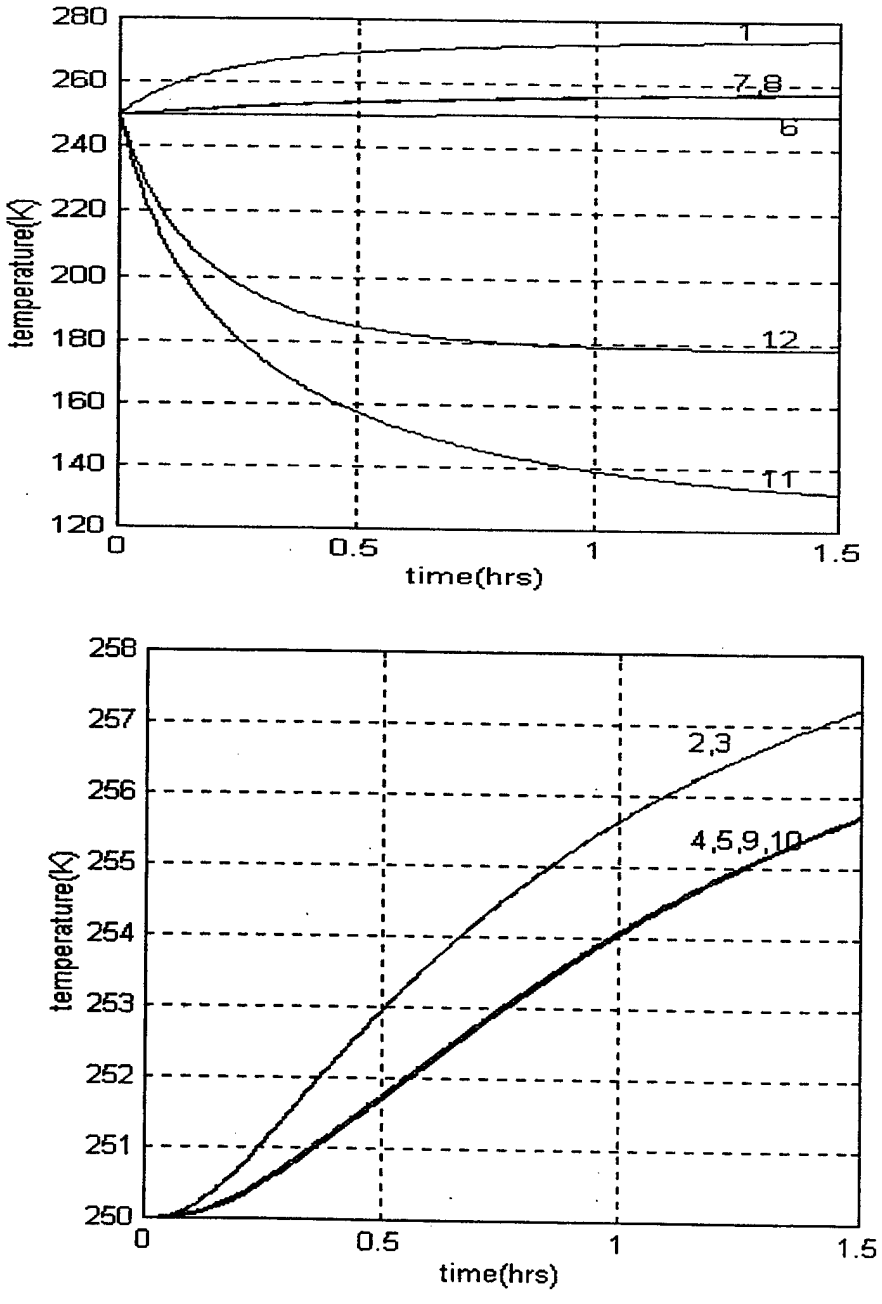

Figure 18. Nodal temperatures vs time. case 2B.

As discussed before with regard to Figure 17 the status of the heaters is fairly inconsequential to the problem, and the temperature-time history is not very different from that in Figure 17. The same reasons are applicable.

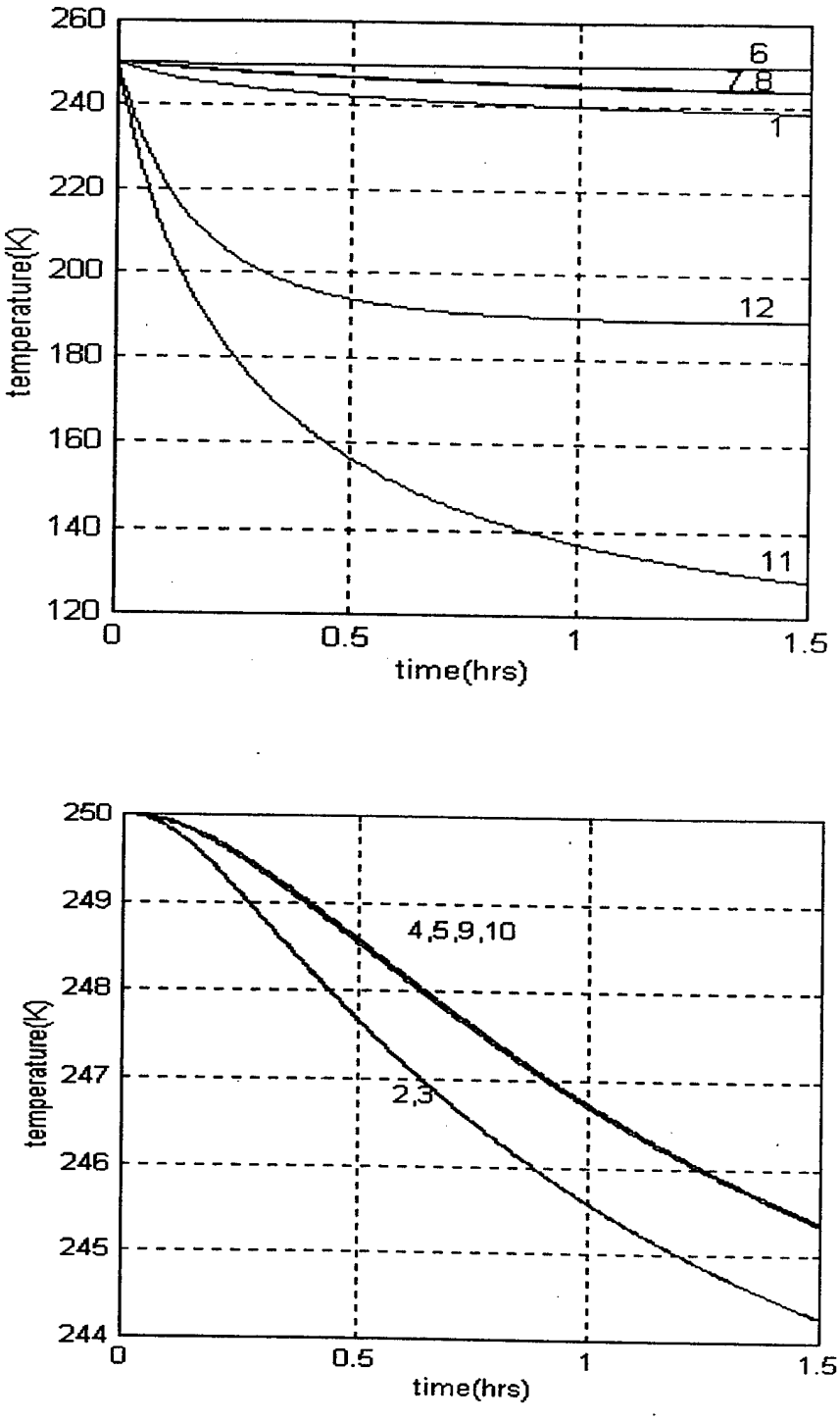

Figure 19. Nodal temperatures vs time. case 3A.

In this case the solar angle of incidence is 90 degrees, i.e. node 1 receives no direct sunlight, while node 11 receives all of the direct sunlight. Consequently the temperature of node 11 is higher, while that of node 1 is lower, than that in Figure 16 for the 45 degree incidence case. Here too the temperature of node 6 remains largely constant.

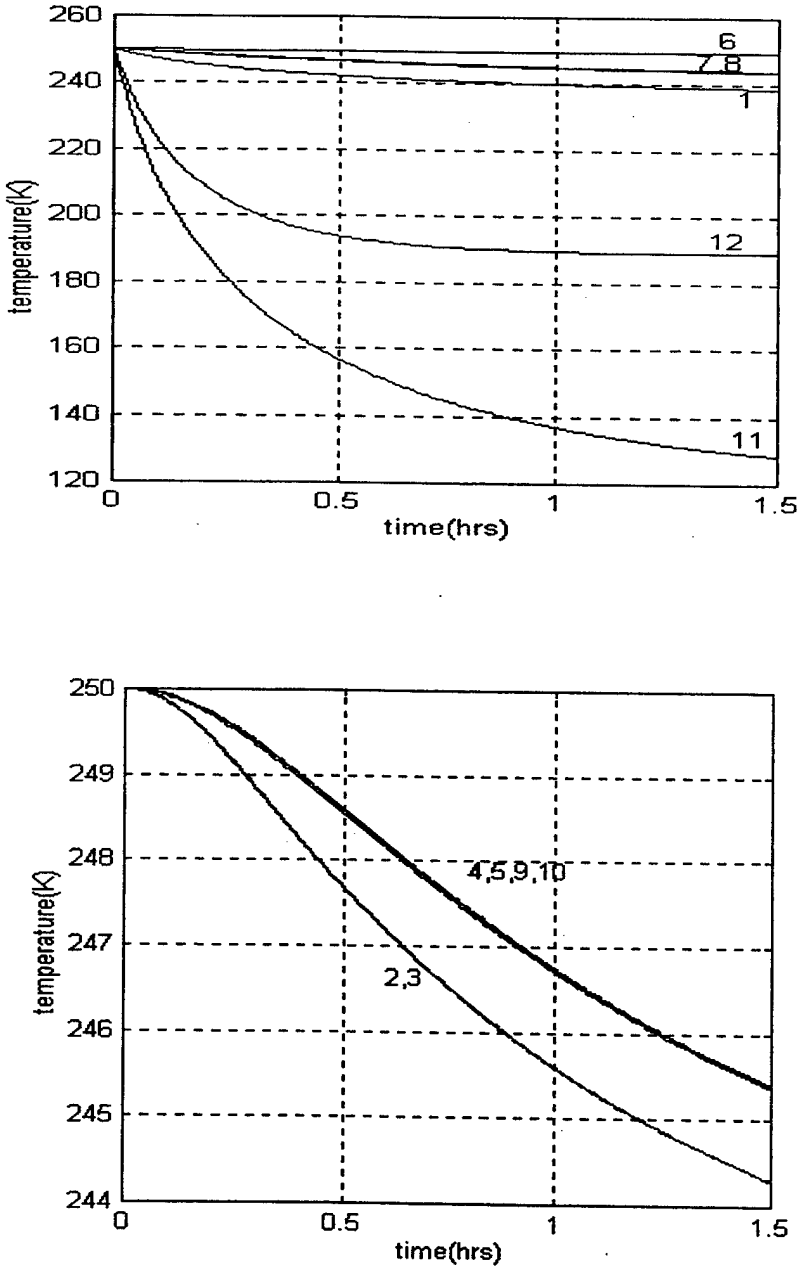

Figure 20. Nodal temperatures vs time. case 3B.

The temperature variation in Figure 20 is similar to Figure 19. The strip heater power has no significant effect on the temperature behavior. The large conductance

between the base and node 6 dominates the energy exchange as discussed earlier. Again the temperature of node 1 and node 6 bound the temperatures all other nodes of PANSAT.

B. PANSAT IN ORBIT

The test cases for PANSAT on orbit are presented in the temperature-time plots below. The first graph shows the temperature external nodes (1,6,7,8,11). The second graph shows the temperature of the internal nodes (2,3,4,5,9,10). The numbers corresponding to the nodal temperature is shown in each figure. The period for PANSAT's orbit is approximately 90 minutes with and eclipse time of 30 minutes.

Also shown are temperature-time plots of the batteries over an extended period (approximately 30 orbits) which show the evolution of the temperature variation to its final periodic state.

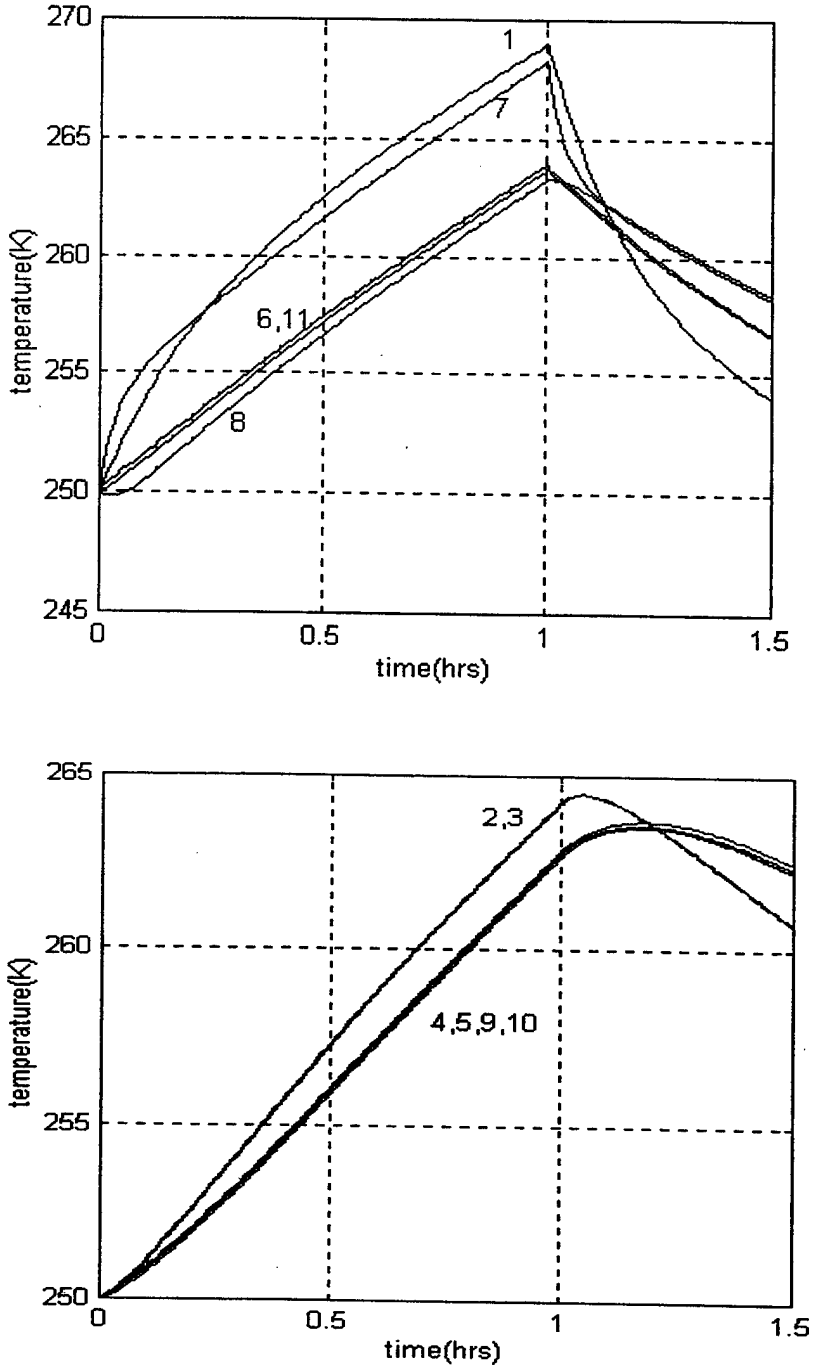

Figure 21. Nodal temperatures vs time. case 4A.

Figure 21 depicts an orientation with node 7 facing the sun. Note that the temperature of node 1 and node 7 are approximately the same value. Nodes 1, 6, and 11 receive both

solar and earth emitted radiation. The temperature of node 1 is eclipsed by the temperature of node 7 for approximately 30 minutes until the effect of the earth emitted radiation causes the temperature of node 1 to surpass the temperature of node 7. Nodes 6 and 11 respond the slowest to temperature gradients in this arrangement.

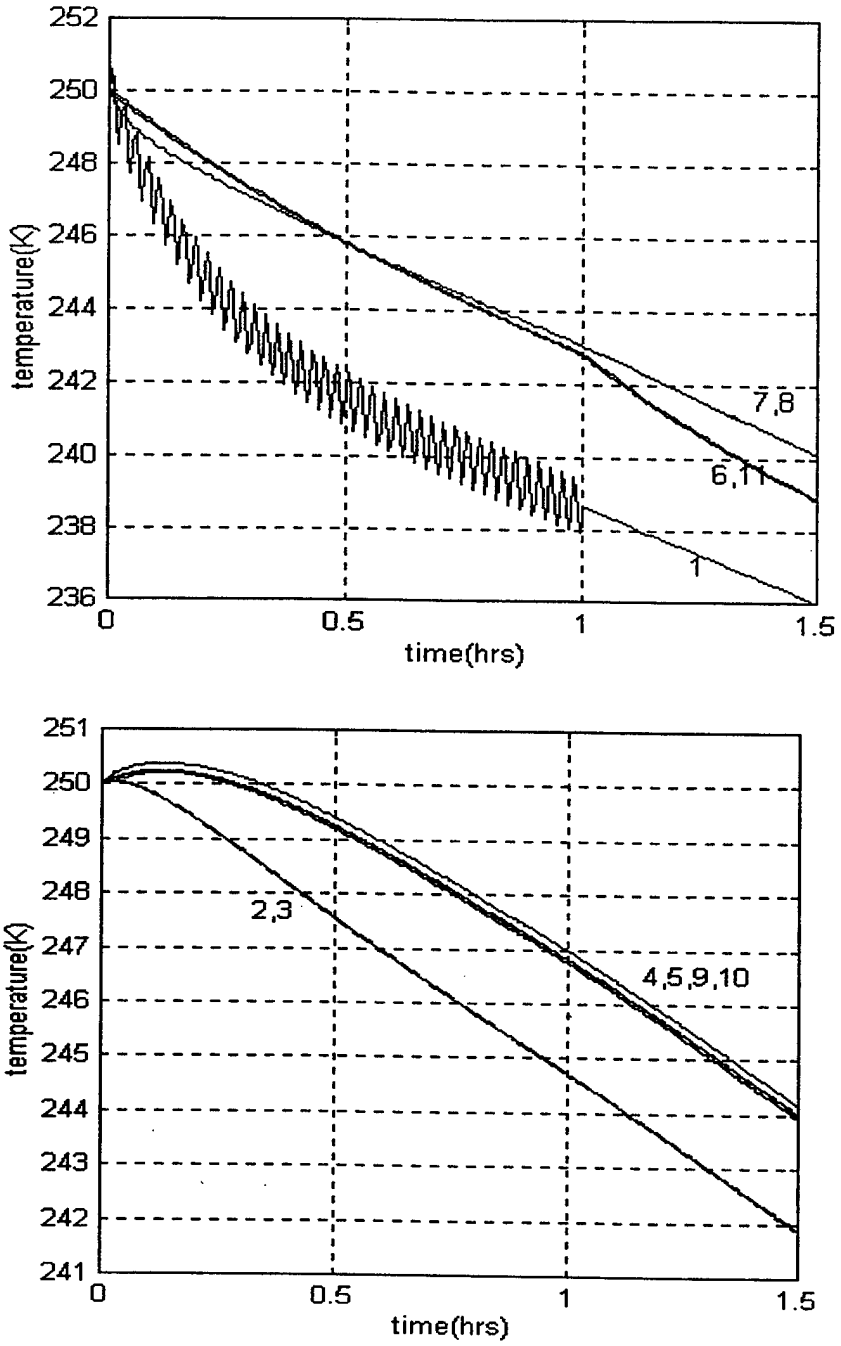

Figure 22. Nodal tempeartures vs time. case 4B

Figure 22 depicts the same general orientation as in Figure 21. PANSAT has a rotation rate of 4 degrees per second. The minimum solar constant value is used and there is no internal heat dissipation. The rotation of the spacecraft minimizes the development of temperature gradients. Hence, the external surfaces of PANSAT radiate heat to cold black space. Again, the time phase lag is evident. The temperature of Node 1 decreases most rapidly. The nodal temperatures are bounded by node 1 and node 6.

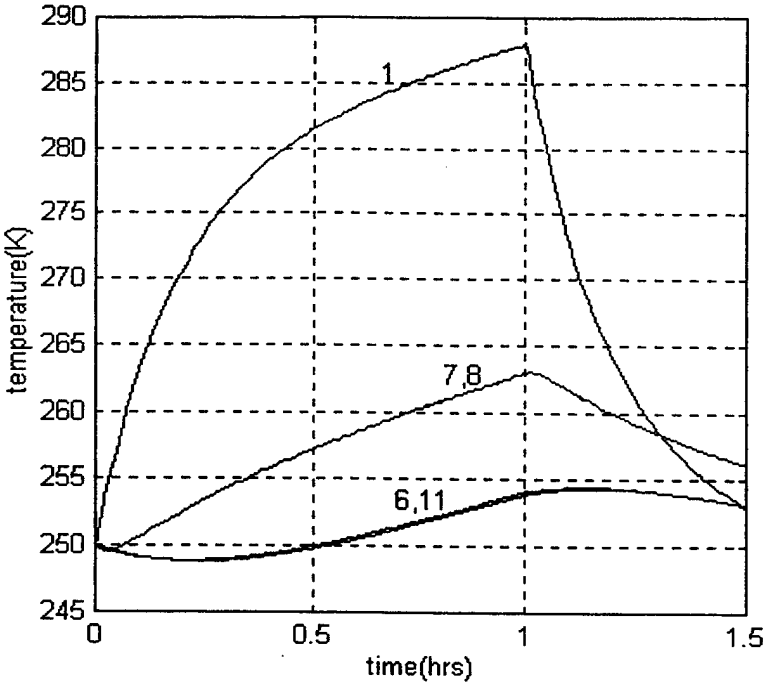

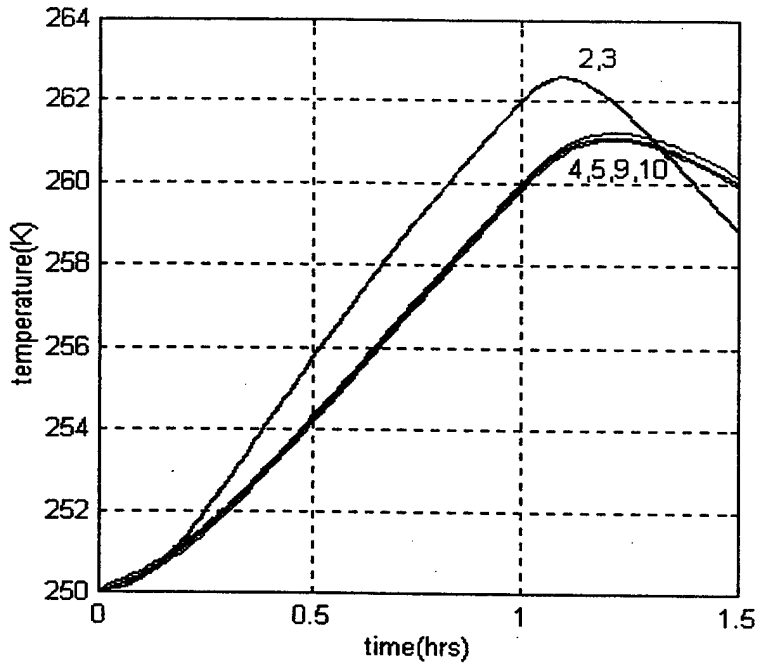

Figure 23. Nodal temperatures vs time. case 5A

Figure 23 depicts the orientation with node 1 facing the sun. Nodes 7 and 8 have approximately equal temperatures values. Since node 1 receives direct sunlight, it reacts more quickly to the temperature gradient. Each of the remaining nodal temperatures exhibit a time-phase lag. The greater the thermal distance between a given node and node 1, the greater the time-phase lag. Thus, node 6 and node 11 have the most pronounced time-phase lag. The temperature of node 1 and 6 acts as a boundary for PANSAT.

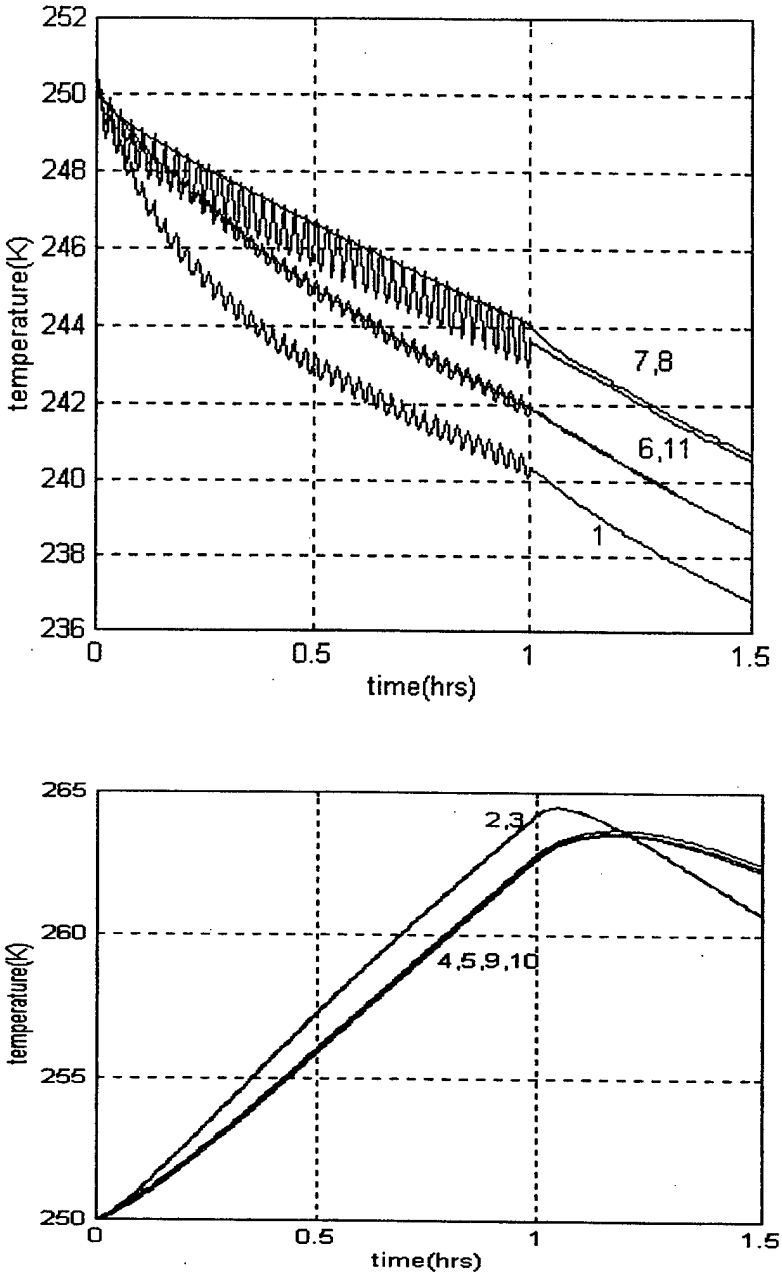

Figure 24. Nodal temperatures vs time. case 5B

Figure 24 depicts the PANSAT with a rotation rate of 4 degrees per second. The results are similar to Figure 22 and the same reasons apply to this case also.

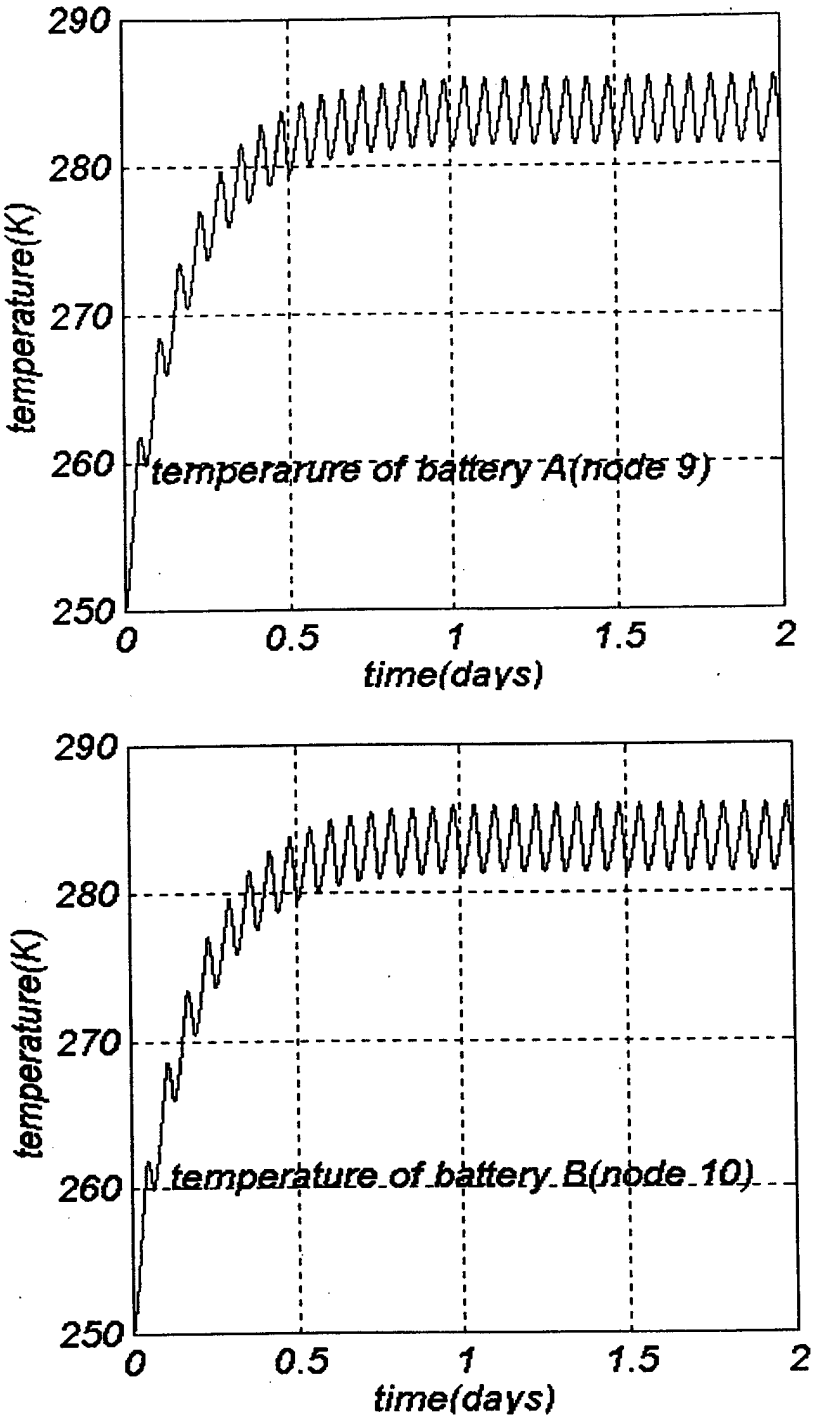

Figure 25. Temperature of Battery A and Battery B vs time. Case 4A

Figure 25 shows the variation of the temperature of the batteries (A and B) over a period of 2 days. In both plots the temperatures reach steady state values in approximately 18 hours and oscillate between 281 K and 286 K with an average temperature of 284 K.

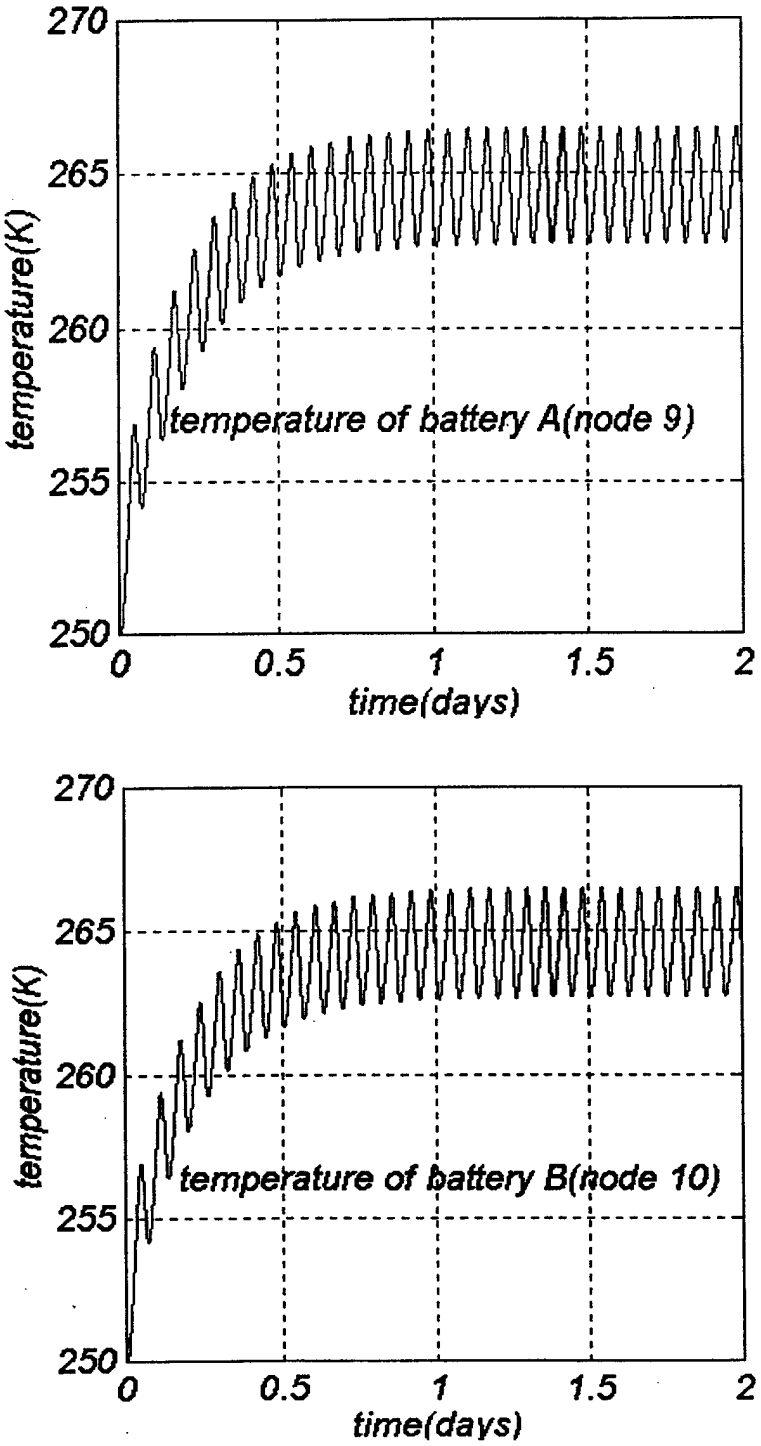

Figure 26. Temperature of Battery A and Battery B vs time. Case 4A

Figure 26 shows the same temperature-time variation as in figure 25. The difference between Figure 25 and Figure 26 is that in this scenario there are no internal heat dissipation from the spacecraft electronic components. Hence, the steady state temperature values are approximately 15 K lower than in the previous case.

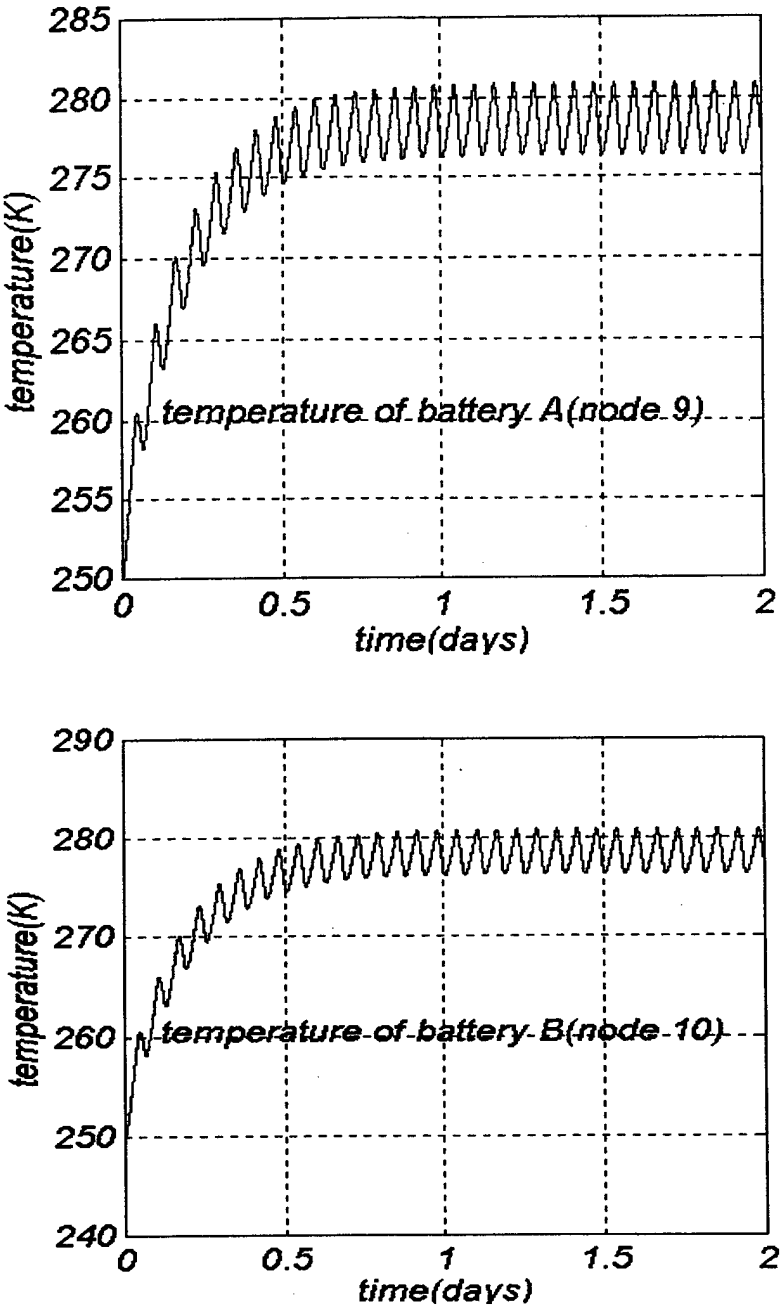

Figure 27. Temperature of battery A and battery A vs time. Case 5A

Figure 27 depicts the temperature for the orientation in case 5A. Again, the temperatures stabililize in approximately 18 hours at a temperature of 278 K.

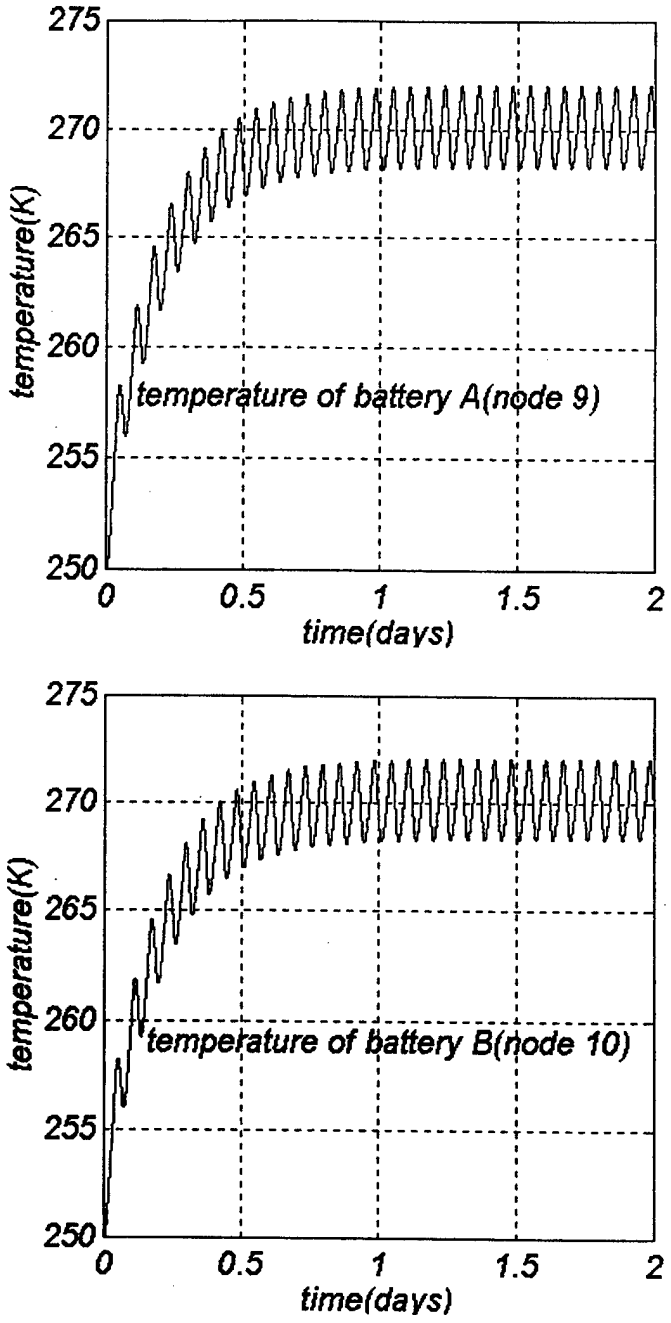

Figure 28. Temperature of battery A and battery A vs time. Case 5A

Figure 28 shows the same scenario as Figure 27 does except that there is no internal heat dissipation in this scenario. A slightly larger temperature difference is observed when there is no internal heat dissipation as compare to the case examined in Figures 25 and 26.

VII. PANSAT THERMAL TESTING

A. THERMAL TESTING IN THE DESIGN PROCESS

Thermal testing is used to verify the design process and increase the confidence in the overall design. System as well as subsystem level testing is conducted. Thermal design is iterative process requiring analysis to improve the thermal performance of the spacecraft. The analytical model is subsequently modified to accurately represent the thermal environment and thermal boundaries.

MIL-STD-1540 B and MIL-STD-343, reference guides for system and component testing, details testing requirements for military spacecraft [Ref. 1]. All test plans will incorporate some elements of this guide. Some tests may not be appropriate for all spacecrafts.

B. SYSTEM LEVEL THERMAL TESTING

A test plan has been developed for PANSAT. It is scheduled to undergo a thermal balance test to validate the thermal analytical model. The thermal balance test will be conducted in conjunction with the thermal vacuum test. This test would normally identify major design errors in the thermal control system [Ref. 7]. Each of the electronic components will undergo thermal testing. The thermal vacuum test verify the proper interaction of components and subsystems.

The number and type of tests conducted vary from spacecraft to spacecraft. Determining the right assortment of tests takes into account the mission's objective, costs, facility availability and schedule.

VIII. CONCLUSIONS

As stated in Chapter I, the emphasis of this analysis was to determine temperature-time history of PANSAT and the temperatures of other key components in PANSAT such as the two Ni-Cd battery compartments. The goal of this work is to ascertain that these temperatures are maintained within their design limits while PANSAT is in a stowed condition awaiting launch and while in orbit. Based on the requirements and assumptions presented in Chapters II and IV respectively, the following conclusions may be made:

A. PANSAT IN THE CANISTER

- In all six cases presented in Chapter V, the battery compartments temperature remain well within the required limit (-30C to +60C).
- The worst scenario for the battery compartments is in cases 3A and 3B for which the solar angle of incidence is 90 degrees and the compartments receive more heat than for the case of normal incidence from directly overhead.
- The base of the GAS canister is thermally large and serves effectively as a heat sink which dominates the thermal behavior of the system by providing a low resistance heat flow path from PANSAT to the rest of the Shuttle.
- The battery compartments exchange more heat by conduction with the lower equipment plate (node 5) than by radiation with the digital control system (node 4) and the mid-deck panels (nodes 7 and 8).
- The kapton strip heaters have a negligible impact on the thermal behavior of PANSAT since the heat that they radiate to node 6 is more easily conducted away through the base, rather than transferred *into* PANSAT.
- The difference between the steady state values and the initial value of the temperatures has a weak dependence on the choice of the initial temperature. This is

because the absolute value of the temperature determines only the radiation conductances which are relatively small. Hence, a different initial temperature effectively results in a corresponding up-down shift in the temperature-time plots discussed earlier.

- Considering the low temperatures experienced by PANSAT while it is stowed in the GAS canister, it'd be desirable to expose PANSAT to a "sun-soak" prior to launch to ensure that the temperatures are closer to the operating values.
- Such a model and the attached program can also be used to simulate cyclic heating/cooling conditions such as those experienced by PANSAT while in orbit. With some modifications the program can also be made to account for the variation of the solar incidence angle (and hence the solar heat input) with time.

B. PANSAT IN ORBIT

The following conclusions can be made for the in-orbit phase of the mission.

- The temperature of node 1 is the highest and the temperature of node 6 is the lowest in both orientations. All other nodal temperatures are within these temperature limits.
- The time phase lag of the temperature response of the nodes verify the accuracy of the model. Nodes (6,11), the furthermost distance from node 1 in exhibit the largest time phase lag and amplitude dampening. Node 11 reacts more slowly than node 6 due to its much larger mass.
- The battery compartment temperatures remain within the specified temperature limits (-5 C to 35 C) for all orientations with no rotation rate.

- This procedure is not dependent on the initial temperature of the nodes. The initial nodal temperatures affect the rise-time to steady state and not the final steady state temperature values.
- Further testing needs to be completed to determine the temperature profile for cases with different rotation rates.
- The temperature profiles of cases 4B and 5B, PANSAT with a rotation rate, exhibit the lowest absolute temperature margins of all the cases. However, the temperature differences is consistent with all of the other cases.
- PANSAT should receive a sun-soak prior to insertion into its orbit to ensure that the initial nodal temperatures are stabilized near normal operating values. This would reduce the time required to bring PANSAT to full operations.

APPENDIX A. NODAL DESCRIPTION

From	To	Conductance [W/K]	Nodal Description
1	8	C_{18}=2.10	For conduction from the top and upper deck panels, and the triangular antenna subassembly panel to the mid-deck panels
1	7	C_{17}=2.10	For conduction from the top and upper deck panels, and the triangular antenna subassembly panels to the mid-deck panels
8	6	C_{86}=2.10	For conduction from the mid-deck panels to the bottom deck panel and lower deck solar panels and the triangular antenna subassembly panels
7	6	C_{76}=2.10	For conduction from the mid-deck panels to the bottom deck panel and the lower deck panels and the 4 triangular antenna subassembly panels
1	2	C_{12}=0.24	For radiation from top and upper deck panels and triangular antenna subassembly panels to the mass storage containers A and B and multiplexer
2	3	C_{23}=126	For conduction from mass storage and multiplexer to the upper equipment plate.
3	4	C_{34}=0.26	For radiation from the upper equipment plate and the electrical power system to the digital control system
4	5	C_{45}=108	For conduction from the digital control system to lower equipment plate and the radio frequency communications

5	6	$C_{56}=0.98$	For conduction from the lower equipment plate and radio frequency communications to lower deck panels and the bottom panel
7	5	$C_{75}=3.50$	For conduction from the mid-deck panels to the lower equipment plate and radio frequency communications
8	5	$C_{85}=3.50$	For transfer by conduction from the mid-deck panels to the lower equipment plate and radio frequency communications
7	9	$C_{79}=0.17$	For radiation from the mid-deck panels to Battery A
9	4	$C_{94}=0.16$	For radiation from battery A to digital control system
10	4	$C_{104}=0.16$	For radiation from battery B to The digital control system
8	10	$C_{810}=0.17$	For radiation from the mid-deck panels to the battery B
7	3	$C_{73}=3.50$	For conduction from the mid-deck panels to upper equipment plate and electrical power system(EPS)
8	3	$C_{83}=3.50$	For conduction from the 4 mid-deck panels to Upper equipment plate and the electrical power system
6	b	$C_{6b}=92$	For conduction from the bottom panel through the Launch vehicle interface to the base of the GAS canister
10	5	$C_{105}=29.8$	For conductance from battery B to the lower equipment plate and the radio frequency communications
9	5	$C_{95}=29.8$	For conductance from battery A to the lower equipment plate and the radio frequency communications

APPENDIX B. NODAL COMPOSITION

Node	Composition	Mass(kg)	Area(m^2)
1	top panel, 4 upper deck panels 4 triangular panels	3.08	0.15
2	mass storage A and B, tmux	2.18	0.03
3	upper equipment plate	2.61	0.06
4	digital control system	4.14	0.04
5	lower equipment plate, radio frequency communications	3.67	0.18
6	bottom panel, 4 lower deck panels, 4 triangular panels	3.08	0.15
7	4 mid-deck panels	1.63	0.07
8	4 mid-deck panels	1.63	0.07
9	battery A	1.97	0.02
10	battery B	1.97	0.02
11	½ GAS canister	1.29	0.14
12	½ GAS canister	1.29	0.14

Node	Composition	Mass(Kg)	Area(m^2)
1	top panel, 4 upper deck panels ,4 triangular panels	3.08	0.15
2	mass storage A and B, tmux	2.18	0.03
3	upper equipment plate, electrical power system	2.61	0.06
4	digital control system	4.14	0.04
5	lower equipment plate, radio frequency communications	3.67	0.18
6	bottom panel, 4 lower deck panels, 4 triangular panels	3.08	0.15
7	4 mid-deck panels	1.63	0.07
8	4 mid-deck panels	1.63	0.07
9	battery A	1.97	0.02
10	battery B	1.97	0.02
11	launch vehicle interface	5.68	0.04

APPENDIX C. PROGRAM CODE

```
% The following code describes a Matlab function used to carry out a transient thermal
analysis of the temperatures of a nodal thermal model of PANSAT. This program is used
for the cases 1A-3A. (PANSAT in the GAS canister)

function  Tdot=thm01(t, T)


%  The inputs 't' and' T' represent the time (to, tf) and the initial  nodal temperature


%%%%%%    all  temperatures are in degrees K      %%%%%%%%%%%%%%%%
% The temperature of the nth node is represented as T(n), n=1..12

% "sig"  below is the Stefan-Boltzmann constant [W/m^2-K^4]
  sig= 5.67e-8;

% emissivity and absorptivity of aluminum (dimensionless)
% assume mass of solar cells much less than underlying aluminum panel

em=0.83;       % emissivity of solar cells
embc=0.88;     % emissivity of beta cloth
emal=0.80;     % emissivity of aluminum
abs=0.78;      % absorptivity of solar cells
absbc=0.30;    % absorptivity of beta cloth
absal=0.30;    % absorptivity of aluminum

% The F's below are the view factors between the different nodes (dimensionless)

F12=0.16;  %assume F21=1
F34=0.63;  %assume F43=1
F79=0.23;  %assume F97=1
F94=0.63;  %assume F49=1
F810=0.23; %assume F108=1
F104=0.63; %assume F410=1
F811=1;
F712=1;
Fh6=0.03;
F6c=0.38;

% masses of nodes [kg]
```

```
m1=3.08;  % mass of node 1
m2=2.18;
m3=2.61;
m4=4.14;
m5=3.67;
m6=3.08;
m7=1.63;
m8=1.63;
m9=1.97;
m10=1.97;
m11=1.29;
m12=1.29;

%%%%%  specific heat capacity of aluminum [J/kg-K]  %%%%%%
Cp=903;

% The A's below are the nodal heat transfer areas [m^2]

A1=0.15;
A6=0.15;
A6b=0.04;
A6c=0.11;      % area of node 6 that sees the can
Ac6=0.60;      % area of  can that sees node 6
A2=0.03;
A3=0.06;
A4=0.04;
A7=0.07;
A8=0.07;
A9=0.02;
A10=0.02;
A11=0.14;
A12=0.14;

% Radiation conductances in the thermal network [W/K] %%%%%%%

C12= (sig*(T(1).^2 + T(2).^2)*(T(1)+T(2))/((1-emal)/(emal*A1) +(1/(A1*F12)) +...
(1-emal)/(emal*A2)));

C34= (sig*(T(3).^2+T(4).^2)*(T(3)+T(4))/((1-emal)/(emal*A3)+(1/A3*F34)+(1-emal)/...
(emal*A4)));

C94=(sig*(T(9).^2+T(4).^2)*(T(9)+T(4))/((1-emal)/(emal *A9) +(1/A9*F94)+(1-emal)/
(emal *A4)));
```

```
C104=(sig*(T(10).^2+T(4).^2)*(T(10)+T(4))/((1-emal)/(emal*A10)+(1/A10*F104)+(1-
emal)/(emal * A4)));

 C79= (sig*(T(7).^2+T(9).^2)*(T(7)+T(9))/((1-emal)/(emal*A7)+(1/A7*F79)...
+(1-emal)/(emal*A9))) ;

C810= (sig*(T(8).^2+T(10).^2)*(T(8)+T(10))/((1-emal)/(emal*A8)+(1/A8*F810)...
+(1-emal)/(emal*A10)));

%  Conduction conductances in the thermal network [W/K]

C23=126;       % node 2 to 3
C18=2.10;      % node 1 to 8
C17=2.10;      % node 1 to 7
C86=2.10;      % node 8 to 6
C76=2.10;      % node 7 to 6
C75=3.50;      % node 7 to 5
C83=3.50;      % node 8 to 3
C73=3.50;      % node 7 to 3
C85=3.50;      % node 8 to 5
C56=0.98;      % node 5 to 6
C45=108;       % node 10 to 8
C6b=92;        % node 6 to base
C95=29.8;      % node 9  to 5
C105=29.8;     % node 10 to 5

% Temperature declarations [K] %%%

 Tinit=250;    % initial temperature of PANSAT prior to opening the Shuttle Hatch
 T_space = 0;  % temperature of space

 Tc6 =.5.*(T(11)+T(12)); %temperature of the part of the canister that sees node6
assumed to be an average of T911) and T(12).

 Tb=Tinit;          % Temperature of the base of the shuttle compartment.
                    % The mass of the base is much larger lvi
%%%%%%%%%%  Heat Input [W]  %%%%%%%%%%%%%%%

qsol=1353;                  % average Solar constant [W/m^2]
theta=pi/2;                 % angle of solar incidence (90 degrees in this example)
Qh=88;                      % input power from all 4 strip heaters to node 6
Qh6in= Qh*abs*Fh6;          % heater input directed to node 6
Q1in=qsol*cos(theta)*A1*abs;
Q11in=qsol*sin(theta)*A11*absbc;
```

```
Q12in=0;

%%%%%%%%%%  Heat Loss [W] %%%%%%%%%%

Q6b=C6b.*(T(6)-Tb);
Q1sp=(em.*sig.*(T(1).^4-T_space.^4)*A1);
Q6c=(sig.*(T(6).^4-Tc6.^4))./((1-em)/(em*A6c) + 1/(A6c*F6c)+(1-emal)/(emal*Ac6));
Q7c=(sig.*(T(7).^4-T(12).^4))./((1-em)/(em*A7) + 1/(A7*F712)+(1-emal)/(emal*A12));
Q8c=(sig.*(T(8).^4-T(11).^4))./((1-em)/(em*A8) + 1/(A8*F811)+(1-emal)/(emal*A11));
Q11sp=embc.* sig.* (T(11).^4-T_space.^4);
Q12sp=embc.* sig.* (T(12).^4-T_space.^4);

%% the differential equations from nodal energy balances %%%%%

Tdot1= -(((C17+C18+C12).*T(1)-C12.*T(2)-C17.*T(7)-C18.*T(8)-
1in+Q1sp)/(m1*Cp));
Tdot2= -((-C12.*T(1)+(C12+C23).*T(2)-C23.*T(3))/(m2*Cp));
Tdot3=-((-C23.*T(2)+(C73+C23+C83+C34).*T(3)-C34.*T(4)-C73.*T(7)-
...C83.*T(8))/(m3*Cp));
Tdot4=-((-C34.*T(3)+(C34+C45+C104+C94).*T(4)-C45.*T(5)-C94.*T(9)-
...C104.*T(10))/(m4*Cp));
Tdot5=-((-C45.*T(4)+(C75+C45+C85+C56).*T(5)-C56.*T(6)-C75.*T(7)-C85.*T(8)-
C95.* ...(T(9)-T(5))-C105.*(T(10)-T(5)))/(m5*Cp));
Tdot6=-((-C76.*T(7)-C86.*T(8)-C56.*T(5)+(C56+C86+C76).*T(6)+Q6b+Q6c-
...Qh6in)/(m6*Cp));
Tdot7=-((-C17.*T(1)-C73.*T(3)-C75.*T(5)-
C76.*T(6)+(C76+C17+C73+C79+C75).*T(7)-C79.* T(9)+Q7c)/(m7*Cp));
Tdot8=-((-C18.*T(1)-C83.*T(3)-C85.*T(5)-C86.*T(6)-
C810.*T(10)+(C85+C18+C83+C86+C810) .*T(8)+Q8c)/(m8*Cp));
Tdot9=-((-C94.*T(4)-C79.*T(7)+(C79+C94).*T(9)+C95.*T(9)-C95.*T(5))/(m9*Cp));
```

```
Tdot10=-((-C104.*T(4)-C810.*T(8)+ (C810+C104).*T(10)+C105.*T(10)-
...C105.*T(5))/(m10*Cp));
Tdot11=-((-Q11in+Q11sp-Q8c)/(m11*Cp));
Tdot12=-((-Q12in+Q12sp-Q7c)/(m12*Cp));

%%%%% now assemble all the Tdot's  into one vector Tdot %%%%%%%%

Tdot=[Tdot1  Tdot2  Tdot3  Tdot4  Tdot5  Tdot6  Tdot7  Tdot8  Tdot9  Tdot10  Tdot11
Tdot12];

% The time integration procedure is now carried out with Tdot as input to the "ode45"
routine in Matlab along with the start and finish times.
```

```
% This program is used for the cases 4A and 4B.

function Tdot=thm21vs(t, T)

%%all temperatures are in degrees K %%%%%%%%%%%%%%

% "sig" is the Stefan-Boltzmann constant (mks units: W/m^2-K^4)
  sig= 5.67e-8;

% emissivity and absorptivity of aluminum (dimensionless)
% assume mass of solar panel much less than underlying panel

em=0.83;
emal=0.80;
abs=0.78;
absal=0.30;

% F's are the view factors (dimensionless)
F12=0.16;  %assume F21=1
F34=0.63;  %assume F43=1
F79=0.23;  %assume F97=1
F94=0.63;  %assume F49=1
F810=0.23; %assume F108=1
F104=0.63; %assume F410=1

% masses of nodes (Kg)

m1=3.08; % mass of node 1
m2=2.18;
m3=2.61;
m4=4.14;
m5=3.67;
m6=3.08;
m7=1.63;
m8=1.63;
m9=1.97;
m10=1.97;
m11=5.68;

%%%specific heat capacity(J/kg-K)%%%%%%%%%%%%%%%%%%%%%%%%%%%%
Cp=903;

% A's are the  nodal areas (in m^2)
```

```
A1=0.15;
A6=0.15;
A6b=0.04;
A2=0.03;
A3=0.06;
A4=0.04;
A7=0.07;
A8=0.07;
A9=0.02;
A10=0.02;
A11=0.17;

%%% radiation conductances in the thermal network (W/K)%%%%%%

% The Temperatures are the Temperatures at a given time "t" %

C12= (sig*(T(1).^2 + T(2).^2)*(T(1)+T(2))/((1-emal)/(emal*A1) +(1/(A1*F12))
+(1-emal)/(emal*A2)));

C34= (sig*(T(3).^2+T(4).^2)*(T(3)+T(4))/((1-emal)/(emal*A3)+(1/A3*F34)+(1-emal)/...
(emal*A4)))

C94= (sig*(T(9).^2+T(4).^2)*(T(9)+T(4))/((1-emal)/(emal *A9) +(1/A9*F94)+(1-
emal)/(emal *A4)));

C104=(sig*(T(10).^2+T(4).^2)*(T(10)+T(4))/((1-emal)/(emal* A10)+(1/A10*F104)+(1-
emal)/(emal * A4)));

C79= (sig*(T(7).^2+T(9).^2)*(T(7)+T(9))/((1-emal)/(emal*A7)+(1/A7*F79)...
+(1-emal)/(emal*A9))) ;

C810=(sig*(T(8).^2+T(10).^2)*(T(8)+T(10))/((1-emal)/(emal*A8)+(1/A8*F810)...
+(1-emal)/(emal*A10)));



% Conduction Conductances in the thermal network (W/K) %%%%%

C23=126;  % node 2 to 3
C18=2.10;  % node 1 to 8
C17=2.10;  % node 1 to 7
C86=2.10;  % node 8 to 6
C76=2.10;  % node 7 to 6
C75=3.50;  % node 7 to 5
C83=3.50;  % node 8 to 3
```

```
C73=3.50;  % node 7 to 3
C85=3.50;  % node 8 to 5
C56=0.98;  % node 5 to 6
C45=108;   % node 10 to 8
C6b=92;    % node 6 to base
C95=29.8;  % node 9  to 5
C105=29.8; % node 10 to 5

%%%Temperature intializations (in K)  %%%%%%%%%%%%%

Tinit=250; %initial temperature of the Pansat prior to opening the Shuttle Hatch

T_space = 0; % Temperature of space


%%%%%%% Heat Input (in W) %%%%%%%%%%%%%%%%%%%%%%%%%%%%%

omega=0;

if t < 3600        % period is approximately 1.5 hrs with
                   % an eclipse time of approximately
                   %  1800sec
 qsol=1399;
 q_albedo=77.1;

else

qsol=0;
q_albedo=0;

 end



theta=0;               % solar angle of incidence
q_earth=32.08;         % earth emitted radiation


Q1in=qsol.* cos(omega.*t)*cos(theta)*A1*abs;
Q6in=(q_earth +q_albedo)*A6*abs;
Q7in=0;
Q8in=0;
Q11in=(q_earth +q_albedo)*(A6b)*absal;
```

```
%%%%%%%%%%equipment power dissipations-W%%%%%%%%%%%%

q_eps=0;  % electrical power system
q_bata=0;  %battery a
q_batb=0;  % battery b
q_rfcomm=0;% Communication system (receiver and transmitter)
q_dcs=0;  % digital control system

%%%%%% Heat Loss (in W) %%%%%%%%%%%%%%%%%%%%%%%%%%%%%%%%%%%%


Q6b=C6b.*(T(6)-T(11));
Q1sp=(em.*sig.*(T(1).^4-T_space.^4)*A1);
Q6sp=(em.*sig.*(T(6).^4-T_space.^4)*A6);
Q7sp=(em.*sig.*(T(7).^4-T_space.^4)*A7);
Q8sp=(em.*sig.*(T(8).^4-T_space.^4)*A8);
Q11sp=(emal.*sig.*(T(11).^4-T_space.^4)*A6b);


%%%%% the differential equations %%%%%%%%%%%%%%%%%%%%%%

Tdot1= -(((C17+C18+C12).*T(1)-C12.*T(2)-C17.*T(7)-C18.*T(8)-
Q1in+Q1sp)/(m1*Cp));

Tdot2= -((-C12.*T(1)+(C12+C23).*T(2)-C23.*T(3))/(m2*Cp));

Tdot3=-((-C23.*T(2)+(C73+C23+C83+C34).*T(3)-C34.*T(4)-C73.*T(7)-C83.*T(8)-
q_eps)/(m3*Cp));

Tdot4= -((-C34.*T(3)+(C34+C45+C104+C94).*T(4)-C45.*T(5)-C94.*T(9)-
C104.*T(10)-q_dcs)/(m4*Cp));

Tdot5= -((-C45.*T(4)+(C75+C45+C85+C56).*T(5)-C56.*T(6)-C75.*T(7)-C85.*T(8)-
C95.* (T(9)-T(5))-C105.*(T(10)-T(5))-q_rfcomm)/(m5*Cp));

Tdot6= -((-C76.*T(7)-C86.*T(8)- C56.*T(5)+(C56+C86+C76).*T(6)+Q6b+Q6sp-
Q6in)/(m6*Cp));

Tdot7=-((-C17.*T(1)-C73.*T(3)-C75.*T(5)-C76.*T(6)+...
(C76+C17+C73+C79+C75).*T(7)-C79.*T(9)-Q7in+Q7sp)/(m7*Cp));

Tdot8=-((-C18.*T(1)-C83.*T(3)-C85.*T(5)-C86.*T(6)-
C810.*T(10)+(C85+C18+C83+C86+C810).*T(8)-Q8in+Q8sp)/(m8*Cp));
```

```
Tdot9=-((-C94.*T(4)-C79.*T(7)+(C79+C94).*T(9)+C95.*T(9)-C95.*T(5)-
q_bata)/(m9*Cp));

Tdot10=-((-C104.*T(4)-C810.*T(8)+ (C810+C104).*T(10)+C105.*T(10)-C105.*T(5)-
q_batb)/(m10*Cp));

Tdot11=-((-Q6b+Q11sp-Q11in)/(m11*Cp));



%%%% now assemble all the "Tdot"s %%%%%%%%%%%%%%%%%%%

Tdot = [Tdot1 Tdot2 Tdot3 Tdot4 Tdot5 Tdot6 Tdot7 Tdot8 Tdot9 Tdot10 Tdot11];


function  Tdot=thm11vs(t, T)

% This program is used for cases 5A and 5B

%%%%%%%%%%%% all temperatures are in degrees K %%%%%%%%%%%%%%

% "sig" is the Stefan-Boltzmann constant (mks units: W/m^2-K^4)
  sig= 5.67e-8;

% emissivity and absorptivity of aluminum (dimensionless)
% assume mass of solar panel much less than underlying panel?
em=0.83;
emal=0.80;
abs=0.78;
absal=0.30;


% F's are the view factors (dimensionless)
F12=0.16;  %assume F21=1
F34=0.63;  %assume F43=1
F79=0.23;  %assume F97=1
F94=0.63;  %assume F49=1
F810=0.23; %assume F108=1
F104=0.63; %assume F410=1
```

```
% masses of nodes (Kg)

m1=3.08; % mass of node 1
m2=2.18;
m3=2.61;
m4=4.14;
m5=3.67;
m6=3.08;
m7=1.63;
m8=1.63;
m9=1.97;
m10=1.97;
m11=5.68;

%%%%%%specific heat capacity(J/kg-K)%%%%%%%%%%%%%%%%%%%%

Cp=903;

%A's are the  nodal areas (in m^2)

A1=0.15;
A1p=0.06;
A6=0.15;
A6b=0.04;
A6p=0.06;
A2=0.03;
A3=0.06;
A4=0.04;
A7=0.07;
A8=0.07;
A9=0.02;
A10=0.02;
A11=0.04;
A11p=0.01;


%%%%%%%Radiation Conductances in the thermal network (W/K) %%%%%%%%%
% The Temperatures are the Temperatures at a given time "t"
%
C12= (sig*(T(1).^2 + T(2).^2)*(T(1)+T(2))/((1-emal)/(emal*A1) +(1/(A1*F12)) +...
(1-emal)/(emal*A2)));
```

```
C34= (sig*(T(3).^2+T(4).^2)*(T(3)+T(4))/((1-emal)/(emal*A3)+(1/A3*F34)+(1-emal)/...
(emal*A4)));

C94= (sig*(T(9).^2+T(4).^2)*(T(9)+T(4))/((1-emal)/(emal *A9) +(1/A9*F94)+(1-
emal)/...(emal *A4)));


C104=(sig*(T(10).^2+T(4).^2)*(T(10)+T(4))/((1-emal)/(emal* A10)+(1/A10*F104)+(1-
emal)/...(emal * A4)));


C79= (sig*(T(7).^2+T(9).^2)*(T(7)+T(9))/((1-emal)/(emal*A7)+(1/A7*F79)...
+(1-emal)/(emal*A9))) ;

C810= (sig*(T(8).^2+T(10).^2)*(T(8)+T(10))/((1-emal)/(emal*A8)+(1/A8*F810)...
+(1-emal)/(emal*A10)));


%%%%% Conduction Conductances in the thermal network (W/K) %%%%%%%%%%

C23=126;  % node 2 to 3
C18=2.10;  % node 1 to 8
C17=2.10;  % node 1 to 7
C86=2.10;  % node 8 to 6
C76=2.10;  % node 7 to 6
C75=3.50;  % node 7 to 5
C83=3.50;  % node 8 to 3
C73=3.50;  % node 7 to 3
C85=3.50;  % node 8 to 5
C56=0.98;  % node 5 to 6
C45=108;  % node 10 to 8
C6b=92;   % node 6 to base
C95=29.8;  % node 9  to 5
C105=29.8; % node 10 to 5

%%%%%%%%%% Temperature intializations (in K) %%%%%%%%%%%%

Tinit=250; %initial temperature of the Pansat prior to departing the shuttle

T_space = 0; % Temperature of space

%%%%%%%%%% equipment power dissipations%%%%%%%%%%%%%%

q_eps=5;  % electrical power system
```

```
q_bata=0; %battery a
q_batb=5; % battery b
q_rfcomm=8;% Communication system (receiver and transmitter)
q_dcs=3;  % digital control system

%%%%%%%% Heat Input (in W) %%%%%%%%%%%%%%%%%%%%%%%%

omega=4*pi/180;   % spin rate for pansat

if t<3600

qsol=1399;
q_albedo=77.1;

else
 qsol=0;
 q_albedo=0;

end

theta=90;

q_earth=32.08;


Q1in=qsol*cos(omega.*t)*sin(theta)*A1p*abs+(q_earth+q_albedo)*A1p*abs;
Q7in=qsol*cos(omega.*t)*sin(theta)*A7*abs;
Q8in=(q_earth+q_albedo)*A8*abs;
Q6in=qsol*cos(omega.*t)*sin(theta)*A6p*abs+(q_earth+q_albedo)*A6p*abs;
Q11in=qsol*cos(omega.*t)*sin(theta)*absal*A11p+(q_earth+q_albedo)*(A11p)*absal;

%%%%%%%%Heat Loss (in W)%%%%%%%%%%%%%%%%%%%%%%%%


Q6b=C6b.*(T(6)-T(11));
Q1sp=(em.*sig.*(T(1).^4-T_space.^4)*A1);
Q6sp=(em.*sig.*(T(6).^4-T_space.^4)*A6);
Q7sp=(em.*sig.*(T(7).^4-T_space.^4)*A7);
Q8sp=(em.*sig.*(T(8).^4-T_space.^4)*A8);
Q11sp=(emal.*sig.*(T(11).^4-T_space.^4)*A6b);


%%%%%%%%  the differential equations %%%%%%%%%%%%%%%%%%%%
```

```
Tdot1= -(((C17+C18+C12).*T(1)-C12.*T(2)-C17.*T(7)-C18.*T(8)-
Q1in+Q1sp)/(m1*Cp));

Tdot2= -((-C12.*T(1)+(C12+C23).*T(2)-C23.*T(3))/(m2*Cp));

Tdot3=-((-C23.*T(2)+(C73+C23+C83+C34).*T(3)-C34.*T(4)-C73.*T(7)-C83.*T(8)-
q_eps)/(m3*Cp));

Tdot4= -((-C34.*T(3)+(C34+C45+C104+C94).*T(4)-C45.*T(5)-C94.*T(9)-
C104.*T(10)-q_dcs)/(m4*Cp));

Tdot5= -((-C45.*T(4)+(C75+C45+C85+C56).*T(5)-C56.*T(6)-C75.*T(7)-C85.*T(8)-
C95.* (T(9)-T(5))-C105.*(T(10)-T(5))-q_rfcomm)/(m5*Cp));


Tdot6= -((-C76.*T(7)-C86.*T(8)-C56.*T(5)+(C56+C86+C76).*T(6)+Q6b+Q6sp-
Q6in)/(m6*Cp));

Tdot7=-((-C17.*T(1)-C73.*T(3)-C75.*T(5)-C76.*T(6)+...
(C76+C17+C73+C79+C75).*T(7)-C79.* T(9)-Q7in+Q7sp)/(m7*Cp));

Tdot8=-((-C18.*T(1)-C83.*T(3)-C85.*T(5)-C86.*T(6)-C810.*T(10)+...
(C85+C18+C83+C86+C810).*T(8)-Q8in+Q8sp)/(m8*Cp));

Tdot9=-((-C94.*T(4)-C79.*T(7)+(C79+C94).*T(9)+C95.*T(9)-C95.*T(5)-
q_bata)/(m9*Cp));

Tdot10=-((-C104.*T(4)-C810.*T(8)+ (C810+C104).*T(10)+C105.*T(10)-C105.*T(5)-
q_batb)/(m10*Cp));

Tdot11=-((-Q6b+Q11sp-Q11in)/(m11*Cp));


%%%%%%%% now assemble all the "Tdot"s %%%%%%%%%%%%%%%%%%%%

Tdot=[Tdot1 Tdot2 Tdot3 Tdot4 Tdot5 Tdot6 Tdot7 Tdot8 Tdot9 Tdot10 Tdot11];
```

REFERENCES

1.Agrawal, Brij.B., *Design of Geosynchronous Spacecraft,* Prentice Hall, Englewood Cliffs, New Jersey 1986, pp. 265-268.

2.Brewster, Quinn M., *Thermal Radiative Transfer and Properties*, John Wiley and Sons, Inc., New York, New York, 1992, pp. 30-37.

3. Chobotov, Vladimir, A., *Orbital Mechanics,* American Institute of Aeronautics and Astronautics, Inc, Washington, DC,1991, pp213.

4.Dewitt, David P. and Incropera, Frank P., *Introduction to Heat Transfer*, John Wiley and Sons Inc., New York, New York, 1996,pp. 315-325.

5.French,James D., Griffin, Micheal, D. , *Space Vehicle Design*, American Institute of Aeronautics and Astronautics, Inc Washington, DC, 1991, pp 371-395.

6. Gilmore, David., *Satellite Thermal Control Handbook,* The Aerospace Corporation Press, El Segundo, CA, 1994, pp 4.19-4.20.

7. Kraus, Allen D. , Thermal Control Of Soacecraft, Department of Electrical and Computer Engineering, Naval Postgraduate School, Monterey, Ca., pp 25-35.

8. Student Edition of Matlab(High-Performance Numeric Computation and Visualization Software) version 4 user's guide, Math Works Inc, Prentice Hall, Englewood cliffs, NJ pp 509.

9.NASA, *Spacecraft Thermal Control, NASA Space Vehicle Design Criteria (Environment),* NASA Technical Information Service, May 1973, pp. 3-17.

10. Pisacane, Vincent, L and Moore, Robert C. ,Fundamentals of Space Systems, Oxford University Press,Inc New York, New York, 1994, pp.433-466.

11. Sampson, Henry, Experimenter's Planning Guide for the Department of defense Space Test Program, The Aerospace Corporation, July 1995, El Segundo,Ca, pp 8-12-8-1.

12. Space System Operations Class 41, Final Report of the First Annual Mission Operations Working Group for the Petite Amateur Navy Satellite (PANSAT), Naval Postgraduate School, June 1995, Monterey,Ca, pp 29-36.

13. Goldstein, Evan , Pallet Ejection System Critical Design Review and Pre-Environmental Test Review September 1997, Swales and Associates Inc Greenbelt, Md., pp31-32.

14. Wertz, James R. and Larson, Wiley J., *Space Mission Analysis and Design*, Kluwer Academic Publishers, Boston , Massachusetts, 1991, pp. 370-386.

INITIAL DISTRIBUTION LIST

1. Defense Technical Information Center.....2
   8725 John J. Kingman Rd., Ste 0944
   Ft. Belvoir, VA 22060-6218

2. Dudley Knox Library 2
   Naval Postgraduate School
   411 Dyer Rd
   Monterey, CA 93943-5101

3. Chairman, Code AA.....1
   Department of Aeronautics and Astronautics
   Naval postgraduate School
   Monterey, CA 93943

4. Professor Ashok Gopinath, Code ME/GK.....1
   Department of Mechanical Engineering
   Naval Postgraduate School
   Monterey, CA 93943

5. Professor Oscar Biblarz, Code AA/Bi.....1
   Department of Aeronautics and Astronautics
   Naval Postgraduate School
   Monterey, CA 93943

6. Chairman, Code SP.....5
   Space Systems Academic Group
   Naval Postgraduate School
   Monterey, CA 93943

7. LT Travis R. Smith.....3
   FACSFAC
   P.O. BOX 357062
   San Diego, CA , 92135-5000